NRC Research Press

ARTICLE

Great Plains polygonal fault system as expressed in Saskatchewan: Late Cretaceous fault initiation and graben formation

Andy St-Onge

Abstract: An extensive polygonal fault system (PFS) has been recognized in fine-grained Late Cretaceous sediments of the Western Interior Seaway of North America. Polygonal fault systems are pervasive organizations of nontectonic faults with fault traces that coalesce to form distinctive polygonal fault patterns. Interpretation of a three-dimensional seismic dataset from southeast Saskatchewan provides insight into fault initiation, timing, and geometry for the Great Plains PFS (GPPFS). Faulting initiates in the Niobrara Formation, with the largest fault throws occurring over Early Cretaceous Viking Formation sandstone accumulations, suggesting that drape compaction over the channel sand initiated some of the faulting. Above this, faulting increases in vertical offset, and the predominant fault strike angles change in the Lea Park, Belly River, and Bearpaw formations (all homotaxial to the Pierre Shale) throughout Campanian time. By late Bearpaw time, the initially almost random fault strike orientations change to well-defined northwest–southeast- and west–east-striking grabens. These grabens have up to 20 m of throw and can be 125 m wide and 900 m long at ~400 m current depth. Predominant graben faults are the continuation of some of the deeper PFS faults. Moreover, the grabens are present over a Campanian clinoform bed and may be interpreted to indicate Bearpaw time extension tectonics that is local or regional in scale. The PFS helps to explain near-surface faulting observed in Late Cretaceous sediments in the Western Interior Seaway and could be used as a model to help explain Late Cretaceous geology, subsurface groundwater flow, and shallow natural gas reservoir continuity.

Résumé : Un vaste système de failles polygonales (SFP) a été relevé dans des sédiments fins du Crétacé tardif de la Voie maritime intérieure de l'Ouest de l'Amérique du Nord. Les SFP sont des organisations pénétrantes de failles non tectoniques dont les traces coalescent pour former des motifs de failles polygonales distinctifs. L'interprétation d'un ensemble de données de sismique tridimensionnelle du sud-est de la Saskatchewan jette un nouvel éclairage sur l'initiation des failles, leur géométrie et le moment de leur formation pour le SFP des grandes plaines (SFPGP). Les failles prennent naissance dans la Formation de Niobrara, les plus grands rejets verticaux se trouvant au-dessus d'accumulations de grès de la Formation crétacée précoce de Viking, ce qui donne à penser que la compaction différentielle au-dessus du cordon sableux est partiellement responsable de l'initiation des failles. Au-dessus, le déplacement vertical le long des failles augmente et les directions prédominantes des failles changent dans les Formations de Lea Park, Belly River et Bearpaw (toutes équivalentes au Shale de Pierre) tout au long du Campanien. Vers la fin du dépôt de la Formation de Bearpaw, les directions des failles, initialement presque aléatoires, changent pour former des grabens bien définis d'orientations nord-ouest–sud-est et ouest–est. Ces grabens ont jusqu'à 20 m de rejet et peuvent atteindre 125 m de largeur et 900 m de longueur à une profondeur actuelle de ~400 m. Les principales failles des grabens sont la continuation de certaines des failles les plus profondes du SFP. Les grabens sont en outre présents au-dessus d'un lit campanien clinoforme et peuvent être interprétés comme indiquant une tectonique d'extension d'échelle locale ou régionale au moment du dépôt de la Formation de Bearpaw. Le SFP aide à expliquer la formation de failles près de la surface observée dans les sédiments crétacés tardifs dans la Voie maritime intérieure de l'Ouest et pourrait être utilisé comme modèle pour aider à expliquer la géologie du Crétacé tardif, l'écoulement de l'eau souterraine et la continuité de réservoirs de gaz naturel peu profonds. [Traduit par la Rédaction]

Introduction

Polygonal fault systems (PFSs) are geological phenomena of coalesced fault traces over a large geographical area. They were first identified by Henriet et al. (1991), interpreting two-dimensional seismic data imaging sediments at an edge of North Sea Basin. The interpretation of over 15 000 km of two-dimensional seismic data resulted in the detailed mapping of fracture patterns in an Eocene clay that extended to outcrop. Fractures and faults with strikes of up to 1 km, throws of up to several meters, and dips from 45° to 80° characterize the faulting. It was interpreted that the faulting occurred shortly after sediment deposition. The term "polygonal fault system" was first used by Cartwright (1994) while examining Cenozoic mudrock sequences in the North Sea. The identification of PFSs has continued since the recognition of the North Sea Basin PFS, especially since the acquisition and use of three-dimensional (3-D) seismic data.

Since 1991, the advent and interpretation of 3-D seismic data have led to the recognition of a few hundred PFSs throughout the world (Cartwright 2014). Cartwright and Dewhurst (1998) outlined seven criteria for PFS identification. One of most obvious characteristics is the polygonal planform geometry of the aggregated fault traces in map view. As the faults grown in vertical offset and lateral position, the fault traces coalesce to form polygonal geometrical patterns that can occur over areas of 150 000 km² or

Received 25 July 2016. Accepted 9 December 2016.

Paper handled by Associate Editor Kathryn M. Bethune.

A. St-Onge. PFS Interpretations Ltd., 427 28th Avenue N.W., Calgary, AB T2M 2K7, Canada.
Email for correspondence: geophysicist@shaw.ca.

more. Another diagnostic observation for PFSs is the existence of layer bound faulting, whereby the strata above and below the faulted zone can be undisturbed (Cartwright and Dewhurst 1998). Individual faults can have 10–100 m of normal throw with 100–1000 m fault spacing. Moreover, the faulting can be divided into two or more tiers of strata, with each tier having independent fault characteristics. Finally, the fault polarity can switch along the vertical extent of a fault.

Fault initiation, fault growth, and the depth of origin of polygonal faults is poorly understood (Cartwright 2014). It is known that the fractures and faults begin in relatively unconsolidated fine-grained mudstones ranging from pure smectitic claystones to almost pure chalks (Cartwright and Dewhurst 1998). Goulty and Swarbrick (2008), Cartwright et al. (2003), and Cartwright (2011) provide overviews of processes that have been examined to explain the fault initiation. Gravitational loading, syneresis (chemically driven volumetric contraction, see Cartwright 2011), sediment density inversion, overpressure, and downslope gravitation sliding have been considered as possible catalysts for fracture initiation. However, there are limitations for each of these processes to be considered a single initiator for all PFSs. The work is still under investigation (Lopez et al. 2015).

Examination of PFS faulting can reveal some characteristics of the underlying sediments. Mattos et al. (2016) discuss the timing of faults and fractures over a salt dome in the Barents Sea northeast of Norway. Jackson et al. (2014) map a change in PFS fault propagation over a slope-fan sandstone on 3-D seismic data imaging sediments from the Måløy slope, offshore Norway. Davies et al. (2009) interpret differential compaction over a rugose opal-A to opal-CT boundary as the fault initiator in an area offshore Norway. Carruthers et al. (2013) map PFS characteristics over salt domes and show that PFS geometries are affected by the deeper diapirs.

The idea of the existence of an extensive PFS in central North America has been presented by the author of this article (St-Onge 2016). The Great Plains PFS (GPPFS) has been identified in Late Cretaceous fine-grained sediments throughout an area shown in Fig. 1. The area was once covered by the Western Interior Seaway (WIS), an epeiric seaway over central North America from Albian to Maastrichtian time (Witzke and Ludvigson 1994). Appalachia to the east and Laramidia to the west were sources for a large amount of fine-grained sediments that were deposited within the seaway (Blakey 2014; Hack 1973).

This work presents an interpretation of part of the GPPFS using a 3-D seismic dataset and well logs from some of the 80 boreholes within the seismic survey area. The data imaged polygonal faulting over Lower Cretaceous Viking Formation sandstone channel accumulations where some early faults (Santonian age) align over the channel. The faulting continues throughout the Cretaceous in two bounded intervals. The deeper interval has a high fault density with small fault offsets and easily mappable planform polygonal patterns of fault traces. The shallower interval has a much lower fault density with larger fault offsets. The final fault geometry for the shallower interval is a strongly oriented set of grabens, ~125 m across, ~900 m long that strike predominantly northwest to southeast and west to east.

The shallowest seismic reflections image faults with the largest amount of vertical offset. The faulting continues above these reflections (which image sediments at ~300 m depth), and can be mapped using the well control. This review will begin with the seismic data interpretation for the deeper, unfaulted Albian sandstones and continue to shallower depths where measured fault densities can reach 10 faults/km^2 for faults with 20 m of maximum throw and 1000 m of fault length.

There are three goals for presenting this research. It is hoped that the paper will garner acceptance for the PFS interpretation for Late Cretaceous sediments deposited within the WIS. A shared interpretation of this PFS should help formulate a better understanding of the morphology of the Upper Cretaceous strata in central North America. Finally, the large number of boreholes within the PFS and the eastern outcrop of the Late Cretaceous should help with PFS interpretations worldwide (St-Onge 2016; Maher 2014; Cartwright 2014).

Fig. 1. Great Plains study area within Canada and the United States showing the Williston Basin outline within the Late Cretaceous Pierre Shale depositional area (modified from Roberts and Kirschbaum 1995).

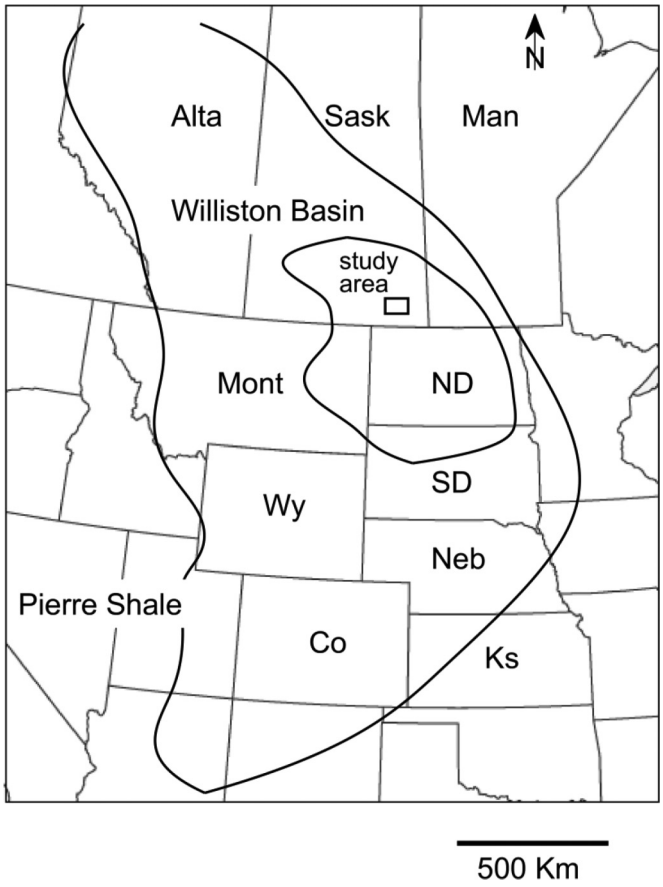

Geologic framework

The Williston Basin is an intracontinental sedimentary basin with a 4900 m depocenter located near Williston, North Dakota (Fig. 1; Anna et al. 2010). The basin primarily consists of Paleozoic carbonate strata and Mesozoic and Cenozoic siliciclastic sediments. The area has been explored for hydrocarbons since the turn of the last century. Commercial oil was found in Manitoba in 1950 and Montana in 1936 (Fischer and Bluemle 1986). The majority of the production in the Williston Basin is from Mississippian-aged carbonate reservoirs and Mississippian–Devonian tight shale–siltstone reservoirs at depths ranging from 450 to ~3400 m. Exploration continues today, with recent activity concentrating on the drilling of the Famennian–Tournasian-age Bakken and Three Forks formations with hydraulically fractured horizontal wellbores.

During the Late Cretaceous, the WIS covered most of central North America including the Williston Basin (Fig. 1). Late Cretaceous sediments were deposited in a single basin over 1000 km wide that extended from the Gulf of Mexico to the Arctic Ocean (Weimer 1960). The western margin of the basin was bounded by highlands produced by the middle Cretaceous Sevier Orogeny, while the eastern margin was relatively stable cratonic lowland (Bertog 2010). Fine-grained strata were sourced from Appalachia to the east and Laramidia to the west deposited between the

Table 1. Stratigraphic chart and PFS observations for this study.

Epoch	Formation	Member	Age	Picks (Ma)	Study area elevation (m)*	Lithology (after Bloch et al. 1999, Christopher et al. 2006, and Christopher and Yurkowski 2004)	PFS comments	PFS fault characteristics			
								Maximum throw (m)	Strike	Average length (m)	Density (faults/km^2)
Early Cretaceous	Pierre Shale Group	Bearpaw	Aquadell	Maastrichtian	72.1		[Aquadell, Cruikshank and Snakebite are				
			Cruikshank				silty claystone, sandstone, iron-rich calcareous sandstone				
			Snakebite				not logged in the study area]				
			Ardkenneth			420	Noncalcareous fine-grained siltstone	Start of borehole logging				
			Beechy		73.3	410	Noncalcareous grey claystone				
			Demaine			381	Grey–brown sandstone with ironstone beds				
			Sherrard	Campanian	74.7	347	Dark grey silty claystone with selenite	[PFS could have caused isopach			
			Matador			295	[Matador, Broderick and Outlook are	variations noted by Christopher			
			Broderick			288	fine-grained units with local thickness variations	and Yurkowski 2004]	23	Aligned	520	~10
			Outlook			254	(see Christopher and Yurkowski 2004)]	Shallowest coherent seismic reflection				
		Belly River			79?	195	Very fine-grained quartzose sandy mudstone	Clinoform bedding; see Fig. 10				
		Lea Park			83.6	153	Grey shale, siltstone, bentonites, fine-grained sandstone	Lower fault density	15	Random	590	1.5
									15	Strongly oriented	420	
	Colorado Group	Niobrara	First White Specks	Santonian	86.3	−1	Grey, speckled, calcareous mudstone and shale	Pervasive faulting, see Fig. 8	11	Oriented	380	10
			Govenlock	Coniacian	89.8	−78	Black bituminous shale and calcareous shale					
		Carlisle					Calcareous shale, argillaceous limestone	PFS begins				
		Morden Shale		Turonian			Black bituminous shale					
		Second White Speckled Shale			93.9	−116	Calcarenite, marlstone, shale, bentonites	Rare, disconnected faulting				
		Belle Fourche					Mudstone to siltstone, bentonites					
		Fish Scales		Cenomanian	100	−191	Claystone to mudstone, basal sandstone, bentonites					
Late Cretaceous		Westgate					Claystone to siltstone					
		Viking		Albian		−210	Coarsening upward fine sandstone	No observed faulting				
		Joli Fou			113	−238	Noncalcareous shale, siltstone, and bentonite interbeds					

Note: Stratigraphic nomenclature, lithology, and PFS characteristics are summarized. Depths are taken from vertical well control located at 49.434°N, −102.634°W.
*Ground elevation = 601 m.

Fig. 2. Viking reflection area under the peak (AUP) map. The AUP bin value is computed by summing the reflection amplitude at each time sample within the interpreted Viking peak reflection. The A–A″ red line locates a west to east seismic line (Fig. 3) and a five-well cross section (Fig. 4). The 1-12-7-6W2 well was drilled at 49.539°N, 102.688°W. The 1 × 1 mile grid is the Dominion Land Survey reference grid. [Colour online.]

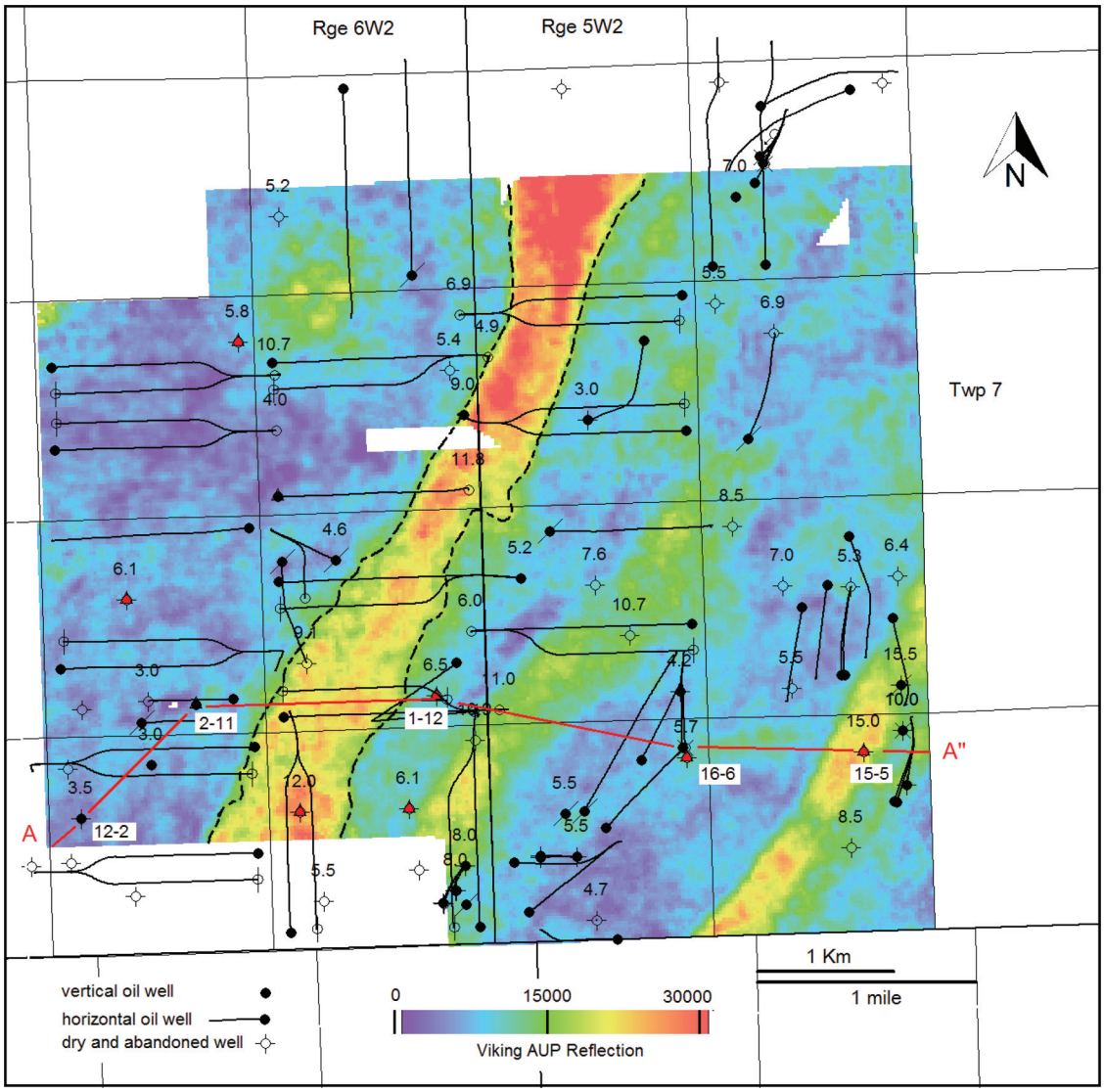

Cenomanian and the Campanian interval during rising and falling sea levels (Schröder-Adams et al. 2001).

In Saskatchewan, the Pierre Shale is divided into the Lea Park, Belly River, and Bearpaw formations, and their fine-grained lithologies are summarized in Table 1. In the study area (Fig. 2), the Cretaceous sediments are overlain by an estimated 30–50 m of glacial till and 50–80 m of Tertiary clastic sediments. This estimation is based on water wells and test wells logged and mapped by the Saskatchewan Water Security Agency (Simpson 1993) just outside the bounds of the 3-D seismic outline. The Cretaceous sediments are ~300 m thick and consist of noncalcareous marine silt and clay (Simpson 1993). The reader is referred to Schultz et al. (1980) for a detailed description of the composition and properties of the Pierre Shale in the Great Plains area. Over half of their 1350 analyzed samples were clay minerals.

The Albian Viking Formation (Bow Island Formation equivalent in Montana and the Muddy Formation equivalent in Wyoming) lies about 180 m below the base of the Pierre Shale in the study area defined by the seismic dataset outlined in Fig. 2. It is a clastic sandstone shale wedge deposited in a near coastal position in western Canada and the northwestern United States (see Walz and Pederson 2013 for a description of a similar depositional environment west of the study area). Inspection of wellbores on or within 3 km of the 3-D seismic outline shown in Fig. 2 showed that the Viking sandstone can be as thick as ~30 m, with porosities ranging from 12% to 27%.

Seismic dataset

The dataset for this study is a 33.3 km² (~12.8 mi²) dynamite 3-D volume with areal coverage as defined by the seismic dataset outline in Fig. 2. The dataset was acquired to image Mississippian-aged carbonate reservoir beds at ~1300 m depth. The study dataset was recorded using vertical component geophones spaced 50 m apart in lines 250 m apart. The dynamite sources, each 0.5 kg, were loaded into 12 m depth tamped holes drilled 50 m apart; the source lines were 350 m apart. The seismic data were processed to a final stacked dataset, and a post-stack time migration was applied before interpretation. The stacked data fold at 1500 m offset was ~25. This fold is more than sufficient to minimize random noise and interbed multiples that are present before the seismic data area stacked. However, the fold of the shallow

Fig. 3. West to east seismic line A–A″ as located in Fig. 2. The Viking reflection peak amplitude increases at the 1-12-7-6W2 and 15-5-7-5W2 locations. There are no faults evident at or below the 2WS reflection. The faulting increases at shallower traveltimes. The synthetic seismic trace is the 1-12-7-6W2 sonic log convolved with a 5/10–60/75 Hz zero-phase wavelet. Note that 1 ms ~ 1 m. [Colour online.]

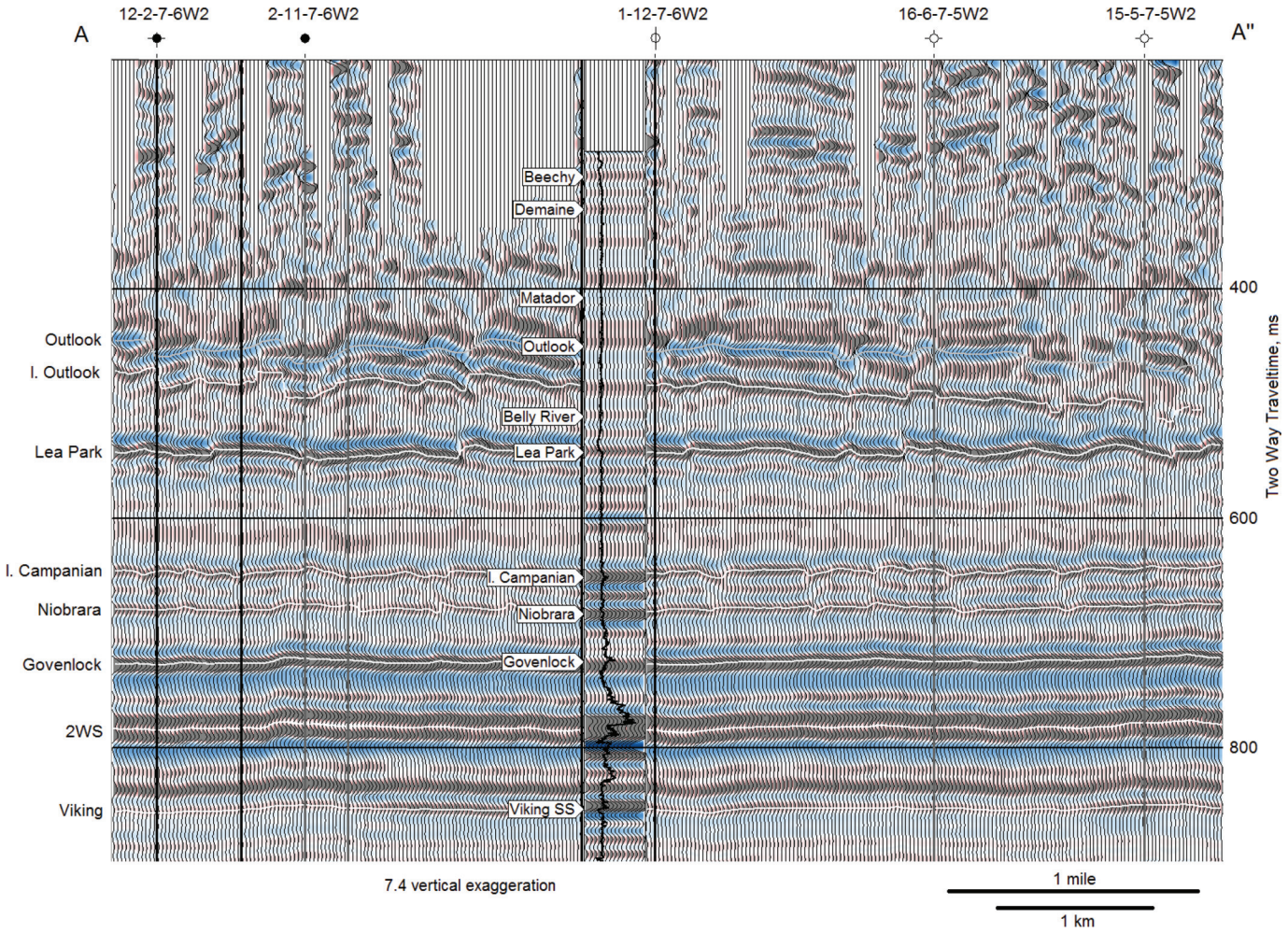

seismic data was low. The calculated fold at the depths examined for this study, specifically 700 m and shallower, was nominal. The stacked seismic data had single-fold coverage until ~300 m depth; three-fold coverage was attained at ~450 m depth and six-fold coverage at ~500 m depth. The low fold at the shallow depths decreases the signal to noise ratio for shallow reflections.

The phase of the seismic data was determined using acoustic impedance as a function of time calculated from the sonic and bulk density logs from the 11-11-7-6W2 wellbore. These impedances were stretched in time ~3% and matched to the seismic dataset using least-squares error estimation. The resulting dataset was phase rotated so that a positive impedance contrast (i.e., low to high velocity with increasing depth) was displayed as a peak reflection. This deterministic phase estimation was verified by performing the same process with a sonic log from 12-1-7-6W2. The verification showed that the phase was within 30° of zero.

A bandpass filter of 6/10–65/80 Hz was applied to the seismic data before they were interpreted and displayed. The deeper, higher fold seismic data have signal frequencies present above 65 Hz. However, the high-end frequency filter enhanced the interpretability for the low-fold shallow reflections. A downside to this is that the bandpass filter limits the resolution of the data. The interval velocity for the seismic data for the shallow reflections down to the Viking reflection is ~2000 m/s. For this discussion, the approximation of 1 ms ~ 1 m will be used. The survey has a dominant frequency of 40 Hz. This implies a dominant wavelength of $\lambda \sim 50$ m (using velocity $v = 2000$ m/s). Zhou and Hatherly (2014) suggest that modern 3-D seismic surveys with computer-aided horizon identification can detect faults with throws as small as $\lambda/16$. This would imply faults less than ~3 m may be difficult to image and interpret in this study.

Observations and data interpretation

Figure 2 is the "area under the peak" (AUP) map for the Viking Formation seismic reflection. The AUP map is computed by summing the reflection amplitudes for each time sample within a specific peak reflection and representing those sums on a scaled colour map. The map can show subtle changes in refection strength from a thin-bed high-velocity zone such as the Viking impedance contrast examined here. The map displays three Viking reflection anomalies across the map striking in a north-northeast direction. The westernmost anomaly is the broadest anomaly at ~500 m in width, and it has the largest computed AUP values, indicating the strongest Viking Formation peak amplitude reflections. The map also shows the 80 horizontal and vertical wells within the boundary of the seismic survey.

Figure 3 displays a seismic line from the dataset that intersects the five-well cross section A–A″ in Fig. 4. The lowermost Viking reflection is unfaulted and has higher amplitude peak reflections along the display that correspond to the high AUP values in Fig. 3. The lower Govenlock and 2WS reflections are relatively higher amplitude, unfaulted events. Both the lower Campanian (l. Campanian)

Fig. 4. Five-well structural cross section A–A″ (see Fig. 2). The mapped seismic reflections have thicker correlation lines.

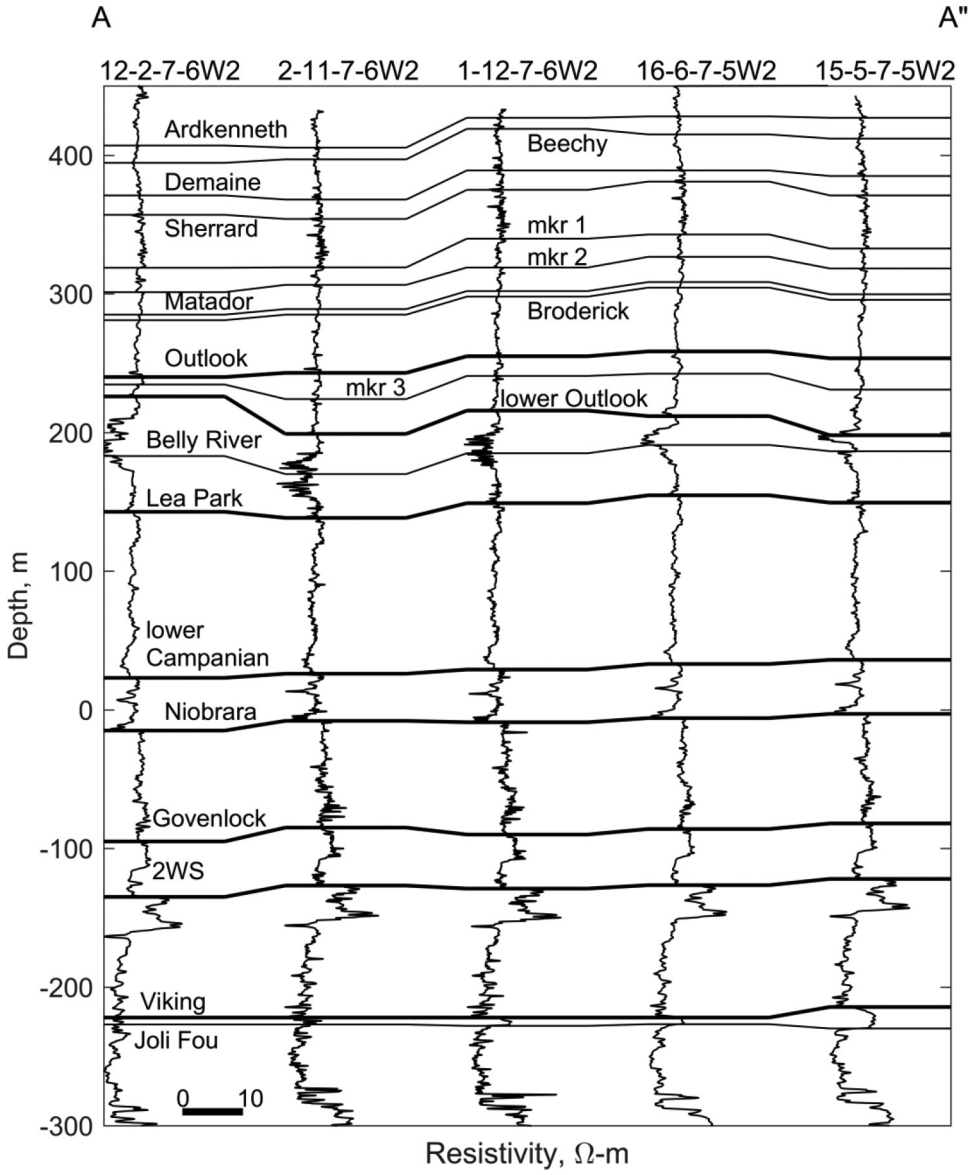

and the Niobrara seismic events are subtle yet continuous strength seismic reflections across the display. An abrupt variation of ~2–3 ms or more for either of these reflections is due to faulting. The most prominent change in either Fig. 3 or 4 is the left to right (west to east) isopach thinning between the lower Outlook (l. Outlook) and Lea Park correlations. The upper correlation is interpreted to be a clinoform bed. Above this, the reflections show increasing faults with larger offset at shallower depths. For example, just west of the 2-11-7-6W2 wellbore, there is a ~15 ms fault that can be interpreted at the lower Outlook member reflection. The Campanian age Beechy, Demaine, and Matador members of the Bearpaw Formation (Fig. 4) are shown on the well tie in Fig. 3 but were not correlated on the seismic data because of absent or discontinuous seismic reflections. Most of the larger structural variations in the geology cross section occur at these shallow depths.

The Viking seismic reflection is sensitive to Viking sandstone thickness variations as shown by crossplotting the Viking sandstone thickness versus the Viking AUP (Fig. 5). Thicker Viking sandstones, as exemplified by 15-5-7-5W2 (Fig. 4), correspond to higher reflection peak amplitudes (Fig. 5). Two of the thicker values in the crossplot (11.8 and 12 m of Viking sandstone thickness)

Fig. 5. Viking sandstone thickness (from well control) and the integrated area under the peak (AUP) crossplot for the Viking peak seismic reflection. R^2, coefficient of determination.

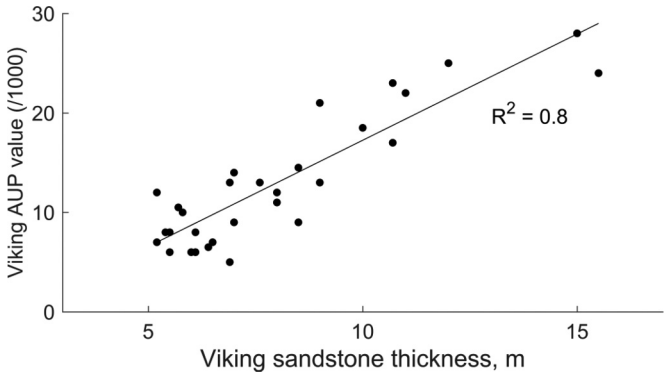

Fig. 6. Isochron (time difference) from the Govenlock to the 2WS. The two 4 ms relative thins (indicated by black arrows) correspond to an area of early PFS faulting and can be seen on the shallower Niobrara gradient map (Fig. 7). Two small 2WS faults are shown (red arrows). [Colour online.]

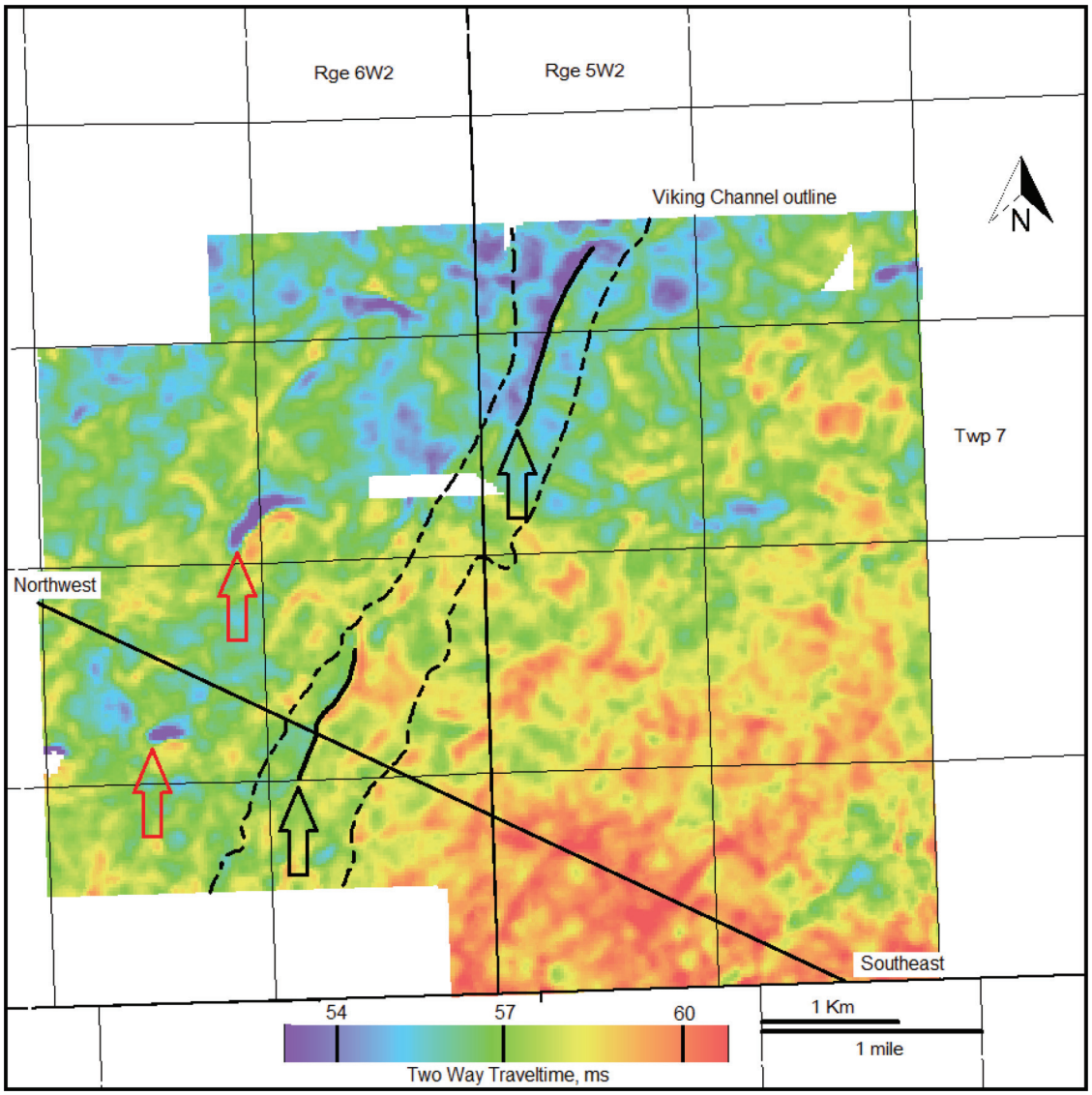

lie within the western seismic anomaly; it is interpreted that this anomaly contains a thicker amount of high-velocity channel sandstones than the other two areas. The dashed outline for this western anomaly is also shown in Figs. 6–9.

Figure 6 is the Govenlock reflection to 2WS reflection isochron map for the survey. Isochron maps display time differences between two reflections on seismic data that can detect subtle isopach variations, especially if the reflections are consistent in character and the interval velocity is constant. The arrows indicate two ~3 ms isochron thins within the outline of the Viking Formation seismic anomaly. These areas are faults that are present in the Govenlock reflection that would have ~3 m of vertical offset. Evidence for drape compaction — a difference in isopach or isochron values that would indicate a lack of sediment compaction at the Viking anomaly — was investigated by constructing, plotting, and interpreting a series of numerous isochron maps. However, no definitive map showing drape compaction was found. Two small anomalies indicated by the red arrows in Fig. 6 mapped 2WS faults. Both locations show 2WS faults with limited lateral extents and about ~2 ms (~2 m) of vertical offset. These faults did not extend higher into the stratigraphic section. There was no observation of 2WS faulting within the bounds of the Viking channel outline.

A gradient map for the Niobrara Formation reflection (Fig. 7) highlights the faulting for that reflection. The map is a Sobel operator edge detection calculation that shows dip magnitude without constructing an isochron map, which may have faulting at both time surfaces. Faulting with the highest amount of vertical offset, about 11 m, is shown with the darkest shading. Most of the longer faults with larger vertical displacement occur in the interior or within 400 m of the interpreted Viking sandstone channel outline. Two of the faults in Fig. 7 occur above the two lines shown in Fig. 6. The average fault offset for the Niobrara reflection is just over 3 ms (or 3 m), and the average fault dip is ~40°. There are ~360 fault traces displayed on the map, which corresponds to a fault density of ~10 faults/km^2 identified within this seismic dataset. Most of the faults are 400 m or less in length, and the longer faults are aligned along the edge or within the outline of the Viking anomaly. There is no evidence for grabens presented on this map, as will be seen for the shallower l. Outlook reflection.

The isochron of the l. Campanian to Niobrara reflections (Fig. 8) shows Niobrara faults in the same position as Fig. 7. The isochron

Fig. 7. Gradient map for the Niobrara seismic reflection. The gradient value *G* is approximated by the sum of two 3 × 3 convolution masks as shown. Also displayed are the planview fault picks for faults that offset sediments from the Niobrara to the l. Campanian (see Fig. 10, dip angles in degrees). The solid black line shows the location of the seismic line discussed in Fig. 10.

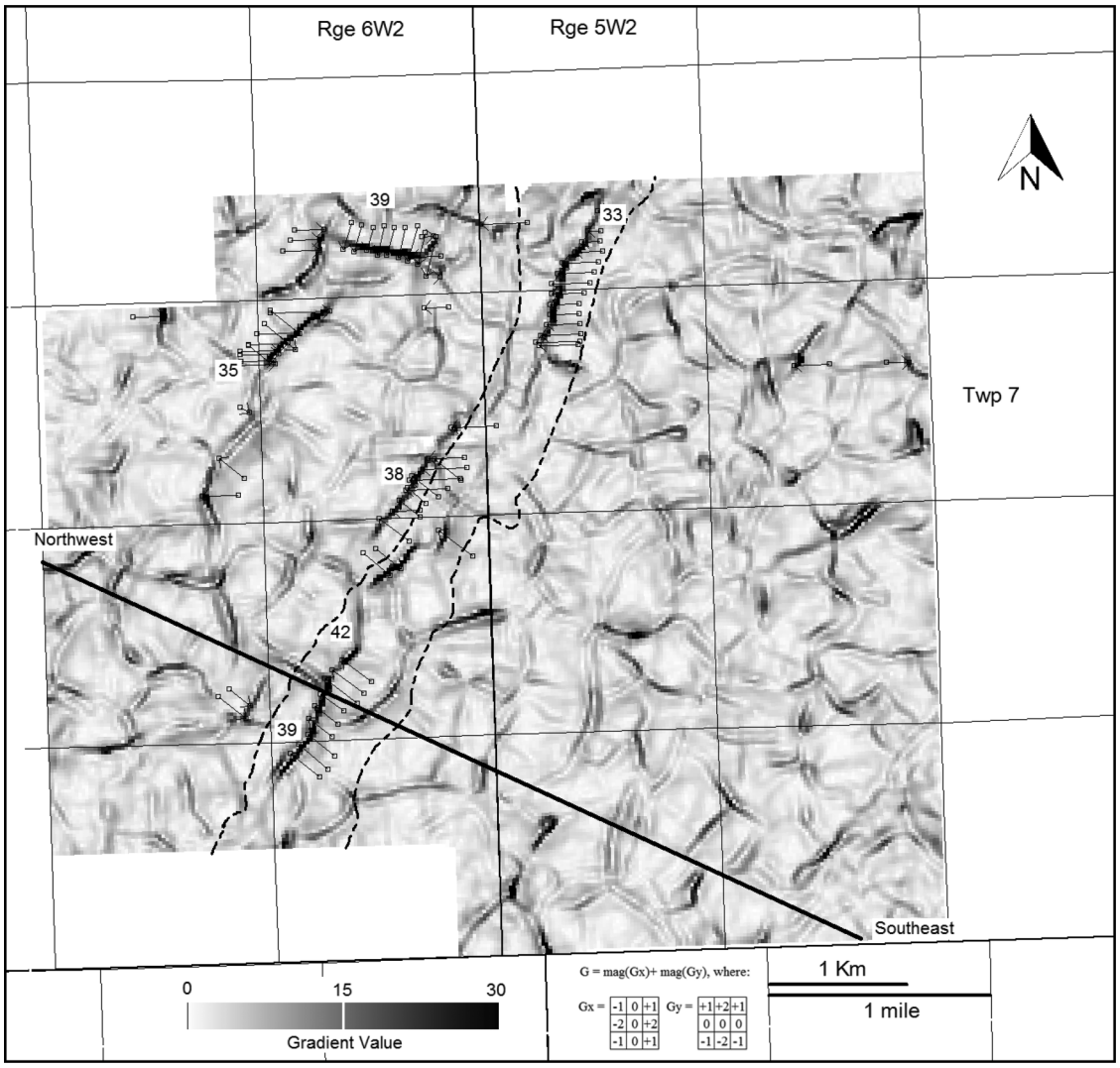

shows more faulting than the gradient map; the additional faults are l. Campanian faults, either as continuation of the Niobrara fault surfaces for larger faults or l. Campanian (and maybe shallower) offsetting faults. The isochron shows little variation in the l. Campanian to Niobrara reflections across the survey other than at the fault traces. Figure 8 shows a definitive polygonal fault pattern that is diagnostic for PFS identification.

Figure 9 shows the gradient map for the Lea Park Formation seismic reflection. There are fewer fault traces shown on this map as compared with the deeper Niobrara reflection (Fig. 7). There are ~55 fault traces displayed on the map (gradient value ≥ 10), which corresponds to a fault density of ~1.5 faults/km² identified within this seismic dataset. Most of the faults are 500 m or more in length, and the longer faults are aligned along the edge or within the outline of the Viking anomaly.

The northwest to southeast seismic line in Fig. 10 (location shown in Figs. 6 and 7) shows a seismic line with the faulting interpreted. The display highlights three salient points for the faulting. Some of the faults are (1) imaged from the Niobrara Formation reflection to shallower than the upper Campanian reflection, (2) only seen on one reflection, and (3) seen on two reflections. Point (4) in Fig. 10 highlights the narrowing time difference within the clinoform between the l. Outlook and Lea Park interpreted seismic reflections. Some of the faults were confined from the Outlook to the Lea Park reflections while others were confined to seismic reflections below the Lea Park reflection. The average dip angle for all faults was just over 40°, but there was an increase in dip angle range of dips for the shallower reflections, as discussed later in the text. Some of the faults shown in Fig. 10 appear to extend to the near surface (not shown) ~300 m above the upper Campanian reflection and within ~100 m of surface. However, it is believed that the low fold of the shallow seismic data makes the fault interpretation questionable for two-way traveltimes less than 400 ms (~300 m depth). Above 300 m depth, the well control was used to search for correlative marker bed variations to infer fault timing.

Figure 11 presents the l. Outlook to Lea Park isochron; these are the two shallowest continuously mappable events across the survey. The west to east isochron thinning is the thinning of a clinoform bed reflection that corresponds to the lower Outlook correlation on the cross section in Fig. 4. The pattern of relative lows across the map is a series of grabens that locally drop the lower Outlook reflection throughout the survey. There are ~30 Campanian grabens (with 10 m or more of local structure) observed on the map, for an average graben count of almost 1 graben/km². The average graben size is 900 m long, 125 m wide, and ~10 m low to adjacent foot-

Fig. 8. Isochron from the l. Campanian to the Niobrara reflections. The thin areas are the fault traces. The polygonal geometry of the fault intersections is the main characteristic for PFSs.

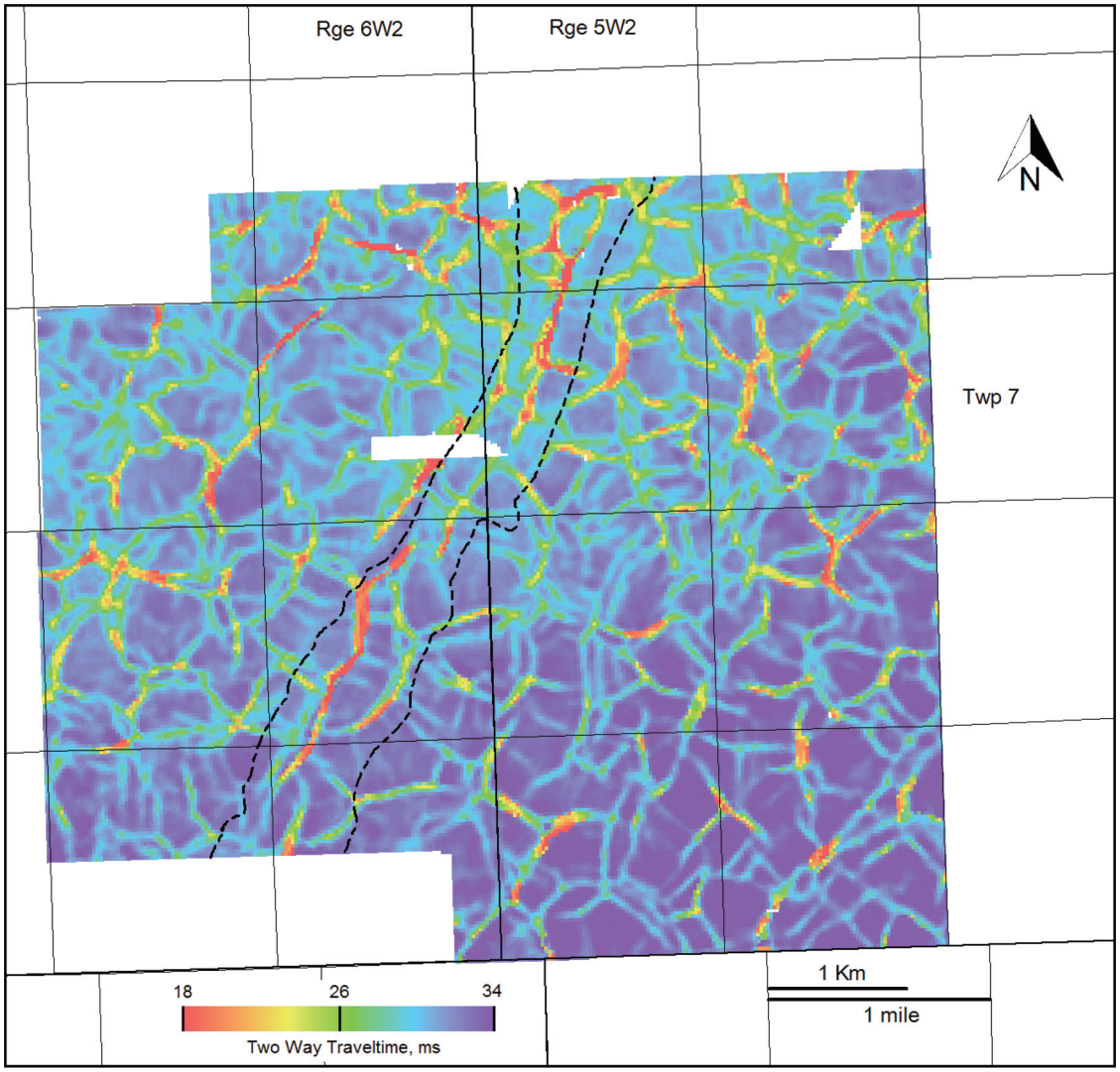

walls. The maximum graben size is 1.5 km long, 200 m wide, and up to 20 m low to adjacent footwalls.

To better display the clinoforms and the grabens shown in Fig. 11, a third-order regional surface was computed for the l. Outlook to Lea Park isochron (Fig. 12). Figure 12 is interpreted to be the regional surface for the clinoform bedding. The surface shown in Fig. 12 dips with values ranging from 0.2° to 0.45°. This map was subtracted from the original isochron in Fig. 11 to highlight the grabens across the survey as shown in Fig. 13. The residual l. Outlook to Lea Park isochron map displays the grabens across the survey; the location of the Viking anomaly is not coincident with these graben alignments. The graben size and their areal density increase on the west side of the survey, and most of the grabens are aligned with the downslope strike of the clinoform anomaly.

Figure 14 presents the fault strike length and directions for the four main seismic reflections. The faulting occurs at many azimuths except for two alignments. The Niobrara faults are either strongly aligned with the western Viking AUP anomaly or appear somewhat random. The l. Campanian and Lea Park seismic reflections have no preferred orientation. The l. Outlook reflection has a strong west to east alignment, and the average strike length has increased compared with the deeper two seismic reflections.

Figure 15 magnifies part of Fig. 4 for the two wellbores on the right side (eastern) of the plot. The comparison was done to try to estimate fault timing for the strata in the two wellbores. Except for late movement of ~20 m for the beds above "mkr 1" in 12-2-7-6W2 and 2-11-7-6W2 (Fig. 4), there is little variation in the correlations above the Demaine marker or below the lower Campanian marker. Using 16-6-7-5W2 as control, the 15-5-7-5W2 resistivity log was cut and adjusted to visually match the two well profiles. No stretching was applied to either log. Eight instances of repeated sections or gaps were noted, including 14 m of missing section at the Outlook correlation in 15-5-7-5W2.

Discussion

This analysis interprets Late Cretaceous sediments using 3-D seismic data tied to well control and presents pervasive faulting that has scant mention in the literature. The faulting has all of the characteristics of a PFS, as outlined by Cartwright and Dewhurst (1998) and summarized earlier in the text. All of the faulting is within fine-grained sediments, which is consistent with PFS formation, namely mudstones, marlstones, interbedded calcarenite, and bentonites, among other lithologies (Christopher et al. 2006). All faults are planar and normal, with fault displacements ranging

Fig. 9. Gradient map for the Lea Park seismic reflection showing the decrease in faulting at the Lea Park level.

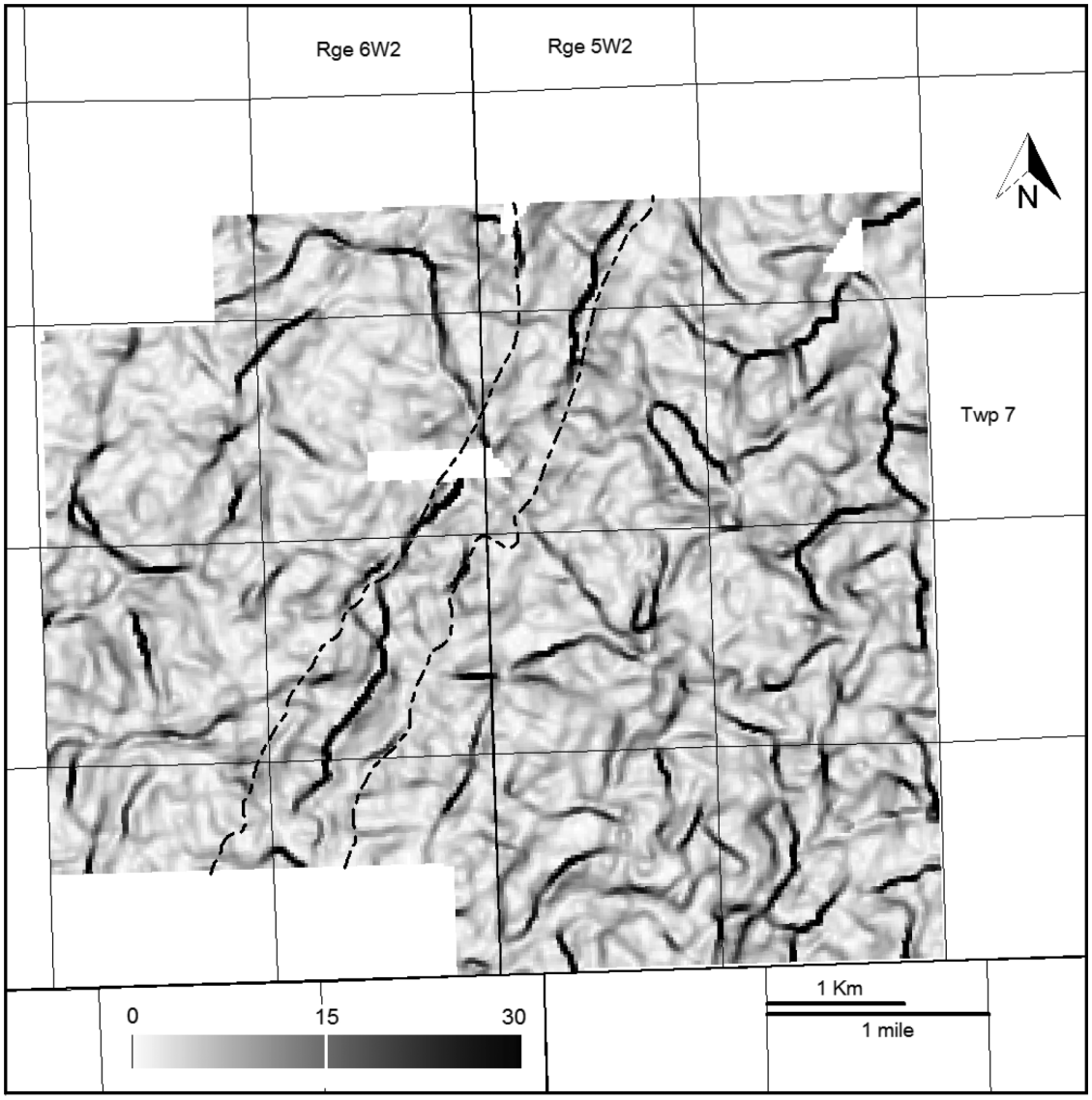

up to 20 m, dips from 25° to 61°, and fault strike lengths up to 1500 m. The GPPFS as discussed by St-Onge (2016) is well represented by the observations presented here. In addition to presenting further evidence for the GPPFS, for this investigation three key points were examined: (1) Can polygonal faults be triggered by subtle variations in underlying sediments? (2) Can we determine the timing of the polygonal faulting? (3) What is causing the formation of grabens?

An examination of the fault strikes and lengths (Fig. 14) for the four key seismic reflections reveal some changes in the PFS characteristics for younger strata. There are two salient summarizing observations: (1) There are more faults with larger offsets at the shallower horizons. (2) The fault strike directions can be strongly aligned or almost random. The deeper Niobrara and l. Campanian reflections image faults that are aligned with the deeper Viking Formation sandstone accumulation or are almost random (Figs. 11, 12). The Lea Park and l. Outlook reflections have consistently longer fault strikes, and the grabens imaged by the l. Outlook reflection are predominantly aligned with a clinoform bed.

Cartwright and Lonergan (1996) describe the geometry and strain characteristics for a Tertiary PFS in the North Sea Basin they interpret as being formed early by fluid expulsion and subsequent shear failure. Their analysis includes a Mohr diagram discussion to demonstrate that pore-pressure increase will induce shear failure before tensile failure because of the low angle of internal friction of the clay-rich sediments. For faulting to occur by shear failure, the principal effective stress has to be reduced by increasing the pore-fluid pressures or by generating tensile stresses by pore-fluid loss, not far-field tectonic stress. The faulting presented here appears to have happened early after deposition; however, I am still working on the mechanism that initiates the pervasive faulting in relatively homogenous fine-grained sediments.

Two factors provided the impetus for the investigating deeper sediments affecting shallower sediment PFS geometries. First, Jackson et al. (2014) map a change in PFS fault propagation over a deeper slope-fan sandstone offshore Norway. Also, Carruthers et al. (2013) show that PFS geometries are affected by deeper salt diapirs in the North Sea Basin. Secondly, it was noticed early in this analysis that the subtle fault traces imaged here on the Govenlock to 2WS isochron map (Fig. 6) are above a Viking reflection anomaly (Fig. 2).

Within the bounds of the dataset, the Viking sandstone developed to 15 m thickness at 15-5-7-5W2 (Fig. 2). The sandstone thickness could be thicker than this on the highest values of the AUP

Fig. 10. Northwest to southeast seismic line (located in Fig. 7) showing some of the faulting complexities imaged with the seismic data. Some faults (1) offset sediments from the Outlook to the Niobrara reflection, while other faults (2) offset individual reflections or (3) offset adjacent reflections. Note the narrowing time difference within the clinoform between the l. Outlook and Lea Park interpreted seismic reflections (4). The thinning Outlook to Lea Park isochron is imaging Bearpaw – Belly River clinoform bedding.

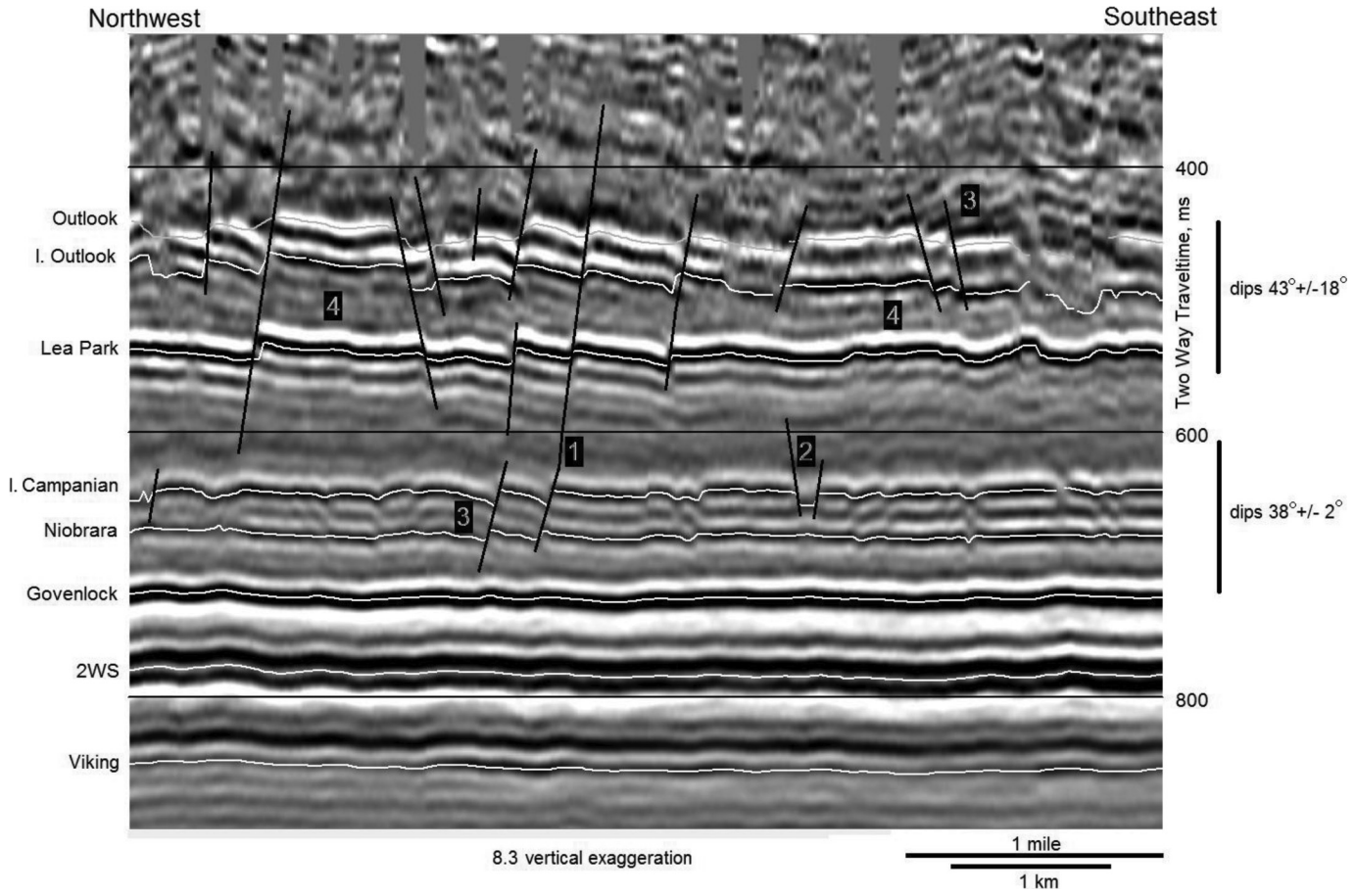

map (Fig. 2), at the north-central portion of the dashed anomaly, but there are no wellbore penetrations in this part of the anomaly to compare with the seismic data. This is where one of the Govenlock faults is observed (Fig. 6).

The AUP–Viking isopach crossplot (Fig. 5) has a high coefficient of determination, $R^2 \sim 0.8$, indicating a good correlation between the Viking sandstone thickness and the AUP map. There could be a number of reasons why this correlation is not stronger. Some data pairs may crossplot off of the best-fit line because of Viking sandstone velocity variations; few of the wells have sonic logs to investigate for variations. The Viking sandstone porosity varies from 12% to 27% for the wellbores within the bounds of the seismic survey; this variability (and effect upon compaction) was not taken into account. Cochran (1991) notes that Viking sandstones could undergo variable compaction, depending upon the amount of chert in the sandstone. Unfortunately, there are no cores from the wellbores in the area to measure Viking chert concentrations. Deviated wellbores were not used to correct downhole coordinated for the crossplot locations (the horizontal wells do not purposely deviate until deeper depths). Bulk density logs were not used to calculate acoustic impedances. The acoustic impedance contrasts could be gradual over a few meters, locally decreasing impedance contrasts. All of these factors could adversely affect the crossplot linearity.

The Govenlock to the 2WS isochron (Fig. 6) shows a few milliseconds of thickening indicative of two faults imaged at the Govenlock reflection and lying above the Viking channel. For drape compaction to have been observed, the compaction would have to have been measureable. The faulting would have to have vertical offset that could be detected by the lower frequency seismic data, on the order of 3 m or more. The faulting would have to have occurred after Viking deposition and before Govenlock deposition. Measurements of the compaction occurring after the Govenlock reflection would have been confused with later faulting.

A gradient map for the Niobrara Formation reflection (Fig. 7) highlights the fault traces for that reflection without relying on an isochron (time difference) between two adjacent surfaces.

The deepest faulting imaged by the seismic dataset are the two small 2WS faults (Fig. 6). No other faulting was observed in the 1800 m of strata deposited below the Viking Formation. Most faulting occurred after deposition of the Govenlock sediments as shown on the five-well cross section (Fig. 4). The faulted Niobrara and the l. Campanian have numerous faults with small amounts of throw and random strikes as well as the Viking anomaly area faults. The chaotic patterns of faulting in these two zones (Figs. 8, 9) are consistent with PFS fault characteristics. Both zones have numerous faults with small amounts of throw and random strikes (except for the Viking channel area faults). Although it appears that the Viking sandstone accumulations affected the PFS faulting, causality can only be inferred, not proven, with this seismic dataset.

Inspection of the data was found to be the best procedure to determine fault timing for the deeper Niobrara and the l. Campanian seismic reflections. The seismic line in Fig. 10 shows a number of faults. Most faults at the Niobrara and l. Campanian reflections occurred after deposition of the Campanian and before deposi-

Fig. 11. Isochron of the l. Outlook to Lea Park reflections. These are the two shallowest continuously mappable events across the survey. The west to east clinoform wedge is apparent, as are the Campanian grabens.

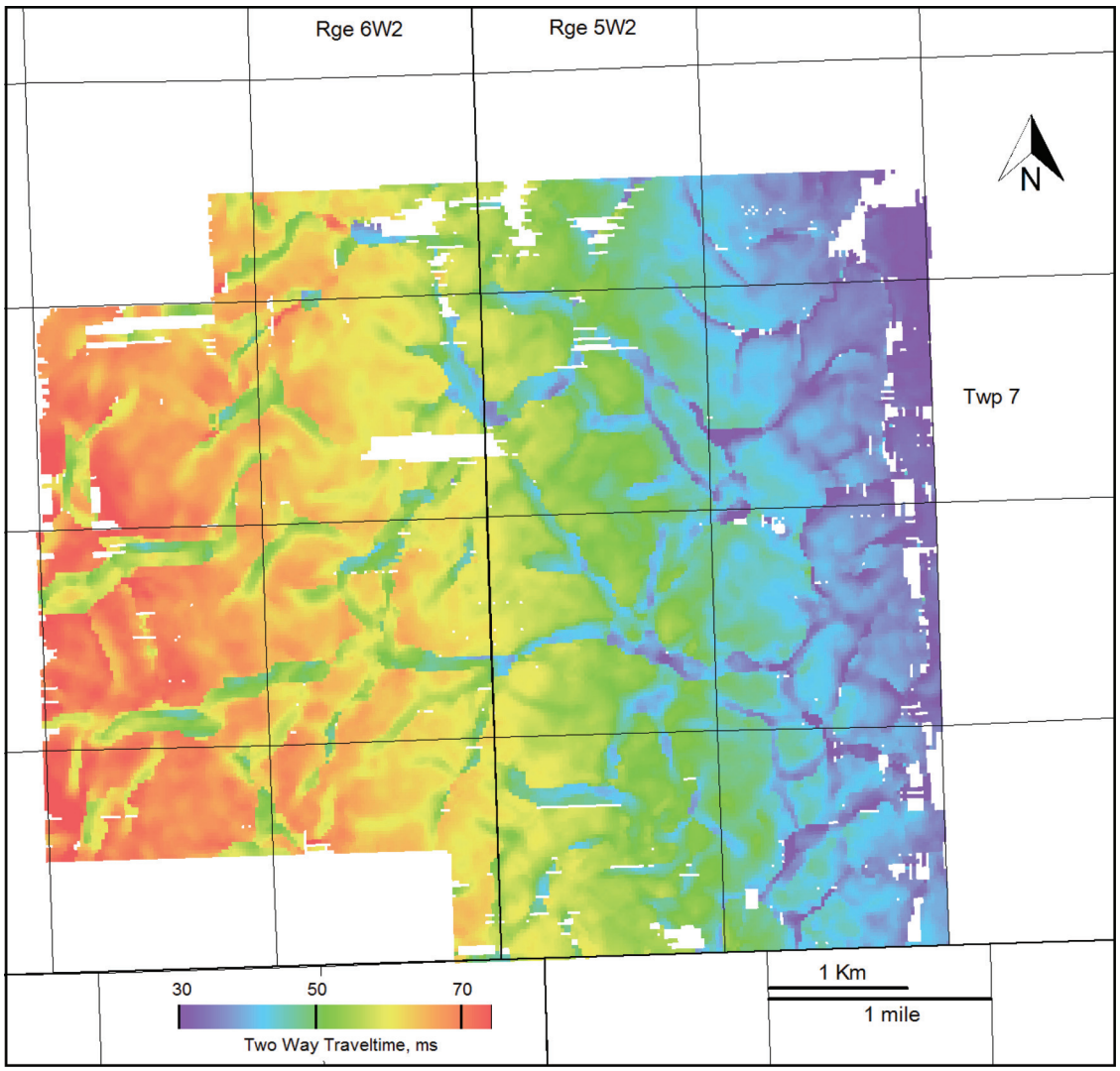

tion of the Lea Park (there is much less faulting at the Lea Park reflection). Unfortunately, there are no impedance contrasts between the Campanian and the Lea Park to better refine the timing of these PFS faults.

The Lea Park gradient map (Fig. 9) shows less faulting, but the faults that are present have more vertical relief than the deeper faults. The faults over the Viking anomaly are still present, but their traces have moved to the northeast along the dip of the fault. The dips for three intervals were measured to look for subvertical faulting. High-angle faults have been observed by others (Tewksbury et al. 2014; Cartwright et al. 2007) in PFSs and are interpreted to be the result of faulting in an overpressured environment. Most of the faulting observed here has a dip ~40°. Visually, the Lea Park faulting (Fig. 9) looks much different than the Niobrara faulting (Fig. 7). It appears that this is mapping a change from the PFS characteristics discussed earlier. The Lea Park gradient map may indicate a change in the PFS faulting characteristics.

The l. Outlook reflection (Figs. 11, 13) images a faulted clinoform surface with superimposed grabens that has little resemblance to a PFS. The surface is a combination of a clinoform bed (Fig. 12) and a graben complex (Fig. 13). Upper Cretaceous clinoforms have been mapped in the WIS. Gendzwill and Stauffer (2007) noted mid- to lower Campanian clinoforms in T34 R28W2 in Saskatchewan, about 350 km northwest of this study area. Hampson (2010) mapped Mancos shale (Campanian) clinoforms in Utah. The clinoform observed here has a maximum thickness of ~70 m (although it could increase in thickness to the west, off of the survey). The clinoform dips range from 0.2° to 0.45°. Patruno et al. (2015) examined and summarized numerous clinoforms and their characteristics. The clinoform presented here correlates with a mud-prone subaqueous delta clinoform.

The clinoform and grabens are the shallowest beds continuously imaged by the 3-D survey (Fig. 10). This is probably due to a lack of shallower impedance contrasts and the low fold of the early seismic data. The grabens on the west side of the survey are deeper and strongly aligned with the downslope strike of the clinoform bed. Compaction of the thicker mud sediments could have resulted in the larger graben offsets. The residual map highlighting the grabens (Fig. 13) has no resemblance to the deeper fault geometries. Any effect of the Viking Formation strata on the faulting geometry has disappeared by late Coniacian time.

An examination of logs from the wellbores can help determine the timing of the graben faults. The five-well cross section and corresponding seismic line (Figs. 3, 4) show a low at the l. Outlook event in 2-11-7-6W2. This wellbore was drilled within the graben shown in Fig. 13 on the west (thicker) side of the mapped clinoform (Fig. 12). The "mkr 3" thickening at 2-11-7-6W2 could be clinoform thinning (compare with 16-6-7-5W2) or indicating the

Fig. 12. Regional surface for the Outlook to Lea Park isochron. This was calculated by fitting a third-order polynomial surface using a least-squares error algorithm to the isochron shown in Fig. 11. [Colour online.]

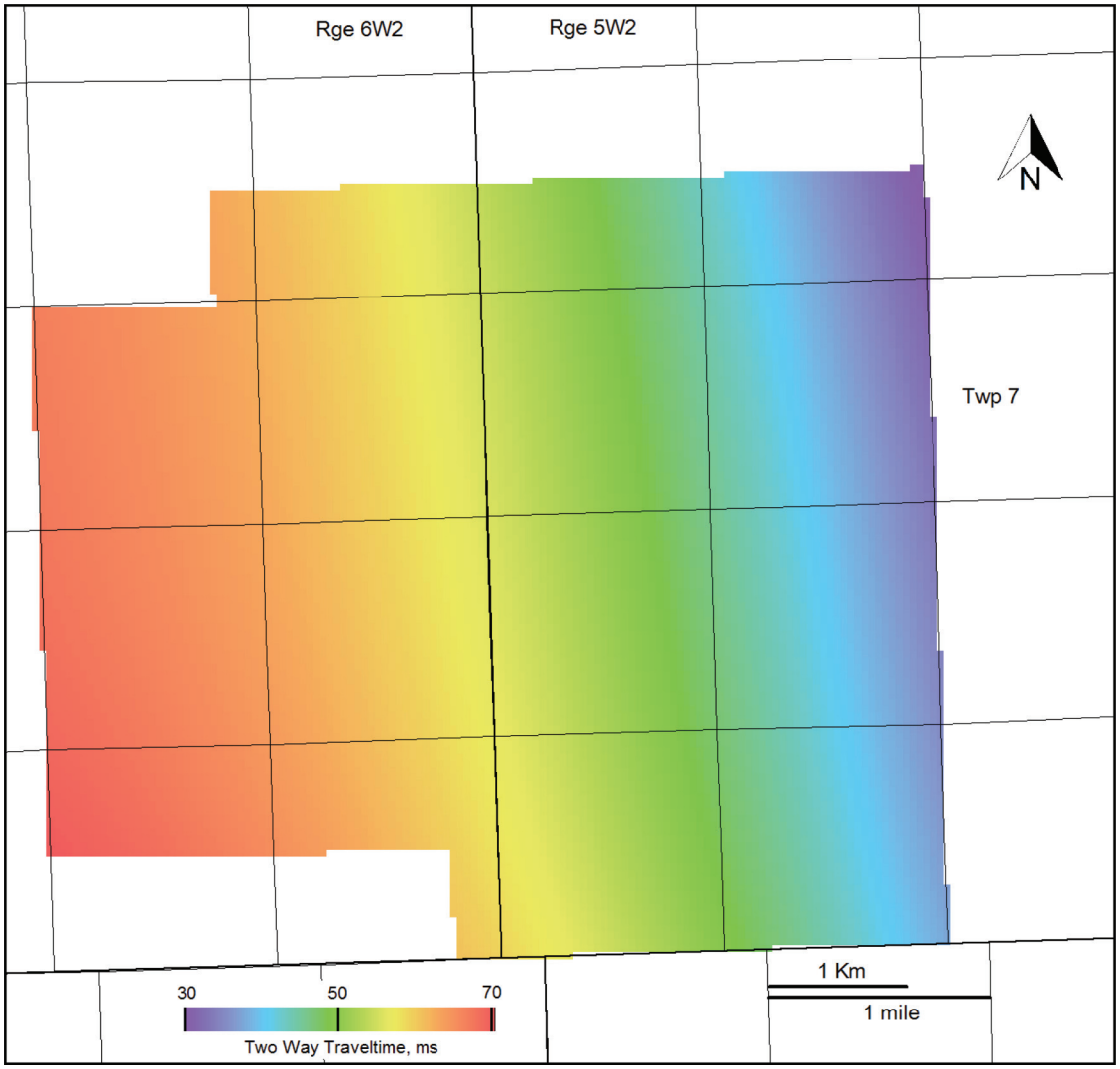

timing of the graben formation. The thickening looks like graben formation on the seismic data (Fig. 3). Also, the beds at 12-2-7-6W2 and 2-11-7-6W2 are depth correlative from the Outlook reflector and shallower, indicating pre-Outlook time (mid-Campanian) graben formation.

Other faulting is evident in Fig. 4. There is an almost uniform drop of ~25 m in the beds from the Ardkenneth to the "mkr 1" at 12-2-7-6W2 and 2-11-7-6W2 relative to the other three wells. There is late movement of these very correlative shallow horizons in these two wellbores. Unfortunately, the log profiles are shown in their entirety (i.e., to wellbore surface casing). The relative low is not observed at the surface where it is covered by ~100 m of Tertiary sediments and glacial till. The timing of these shallow faults cannot be determined with the seismic data because of the absence of shallow reflections.

There are some inconsistent correlations in Fig. 4. This could be due to syndepositional faulting affecting the lithology. Consider Fig. 15, which shows 16-6-7-5W2 as a reference wellbore for 15-5-7-5W2; the wellbores are 1300 m apart. The 15-5 resistivity log was broken down into the largest possible correlative sections as compared with the 16-6 wellbore. The amount of missing and overlap section suggests complicated geology that can be caused by faulting. Moreover, the seismic data images a large amount of faulting that is not sampled at the well locations, indicating that the drilling density aliases the geology, meaning the subsurface faulting down to the 2WS is underestimated by the well control.

Bellahsen and Daniel (2005) examined fault reactivation of normal faults in a different orientation to existing faults using physical models. They found that the orientation of the pre-existing discontinuities strongly influence the evolution through time of the fault orientation distribution. Their physical models had well-defined strikes for the lower faults; this enables fault orientation distribution causality to be examined. The randomness of the PFS faulting below the graben system does not allow for this examination. Reeve et al. (2015) examined the growth of noncollinear normal fault system interpreting 3-D seismic data at the Malloy Slope area of the North Sea. They noted that pre-existing weaknesses are important. In this study, some of the Coniacian PFS faults remained active or reactivated and continued vertically through Campanian time.

Late Cretaceous grabens have been noted in other areas of the WIS. St-Onge (2016) presents a graben map with well-defined strikes in an area 90 km southeast of this study area. Nurhasan and Davis (2016) present a map showing well-defined grabens in the Pierre Shale in the Denver Basin northeast of Boulder, Colorado, where the Niobrara Formation grabens are of the same magnitude as those presented here — 300–450 m wide, 1.5 km long wide, and 9–40 m deep. They interpret these grabens to be the

Fig. 13. Residual for the Outlook to Lea Park isochron calculated by subtracting the map in Fig. 11 from the map in Fig. 12. [Colour online.]

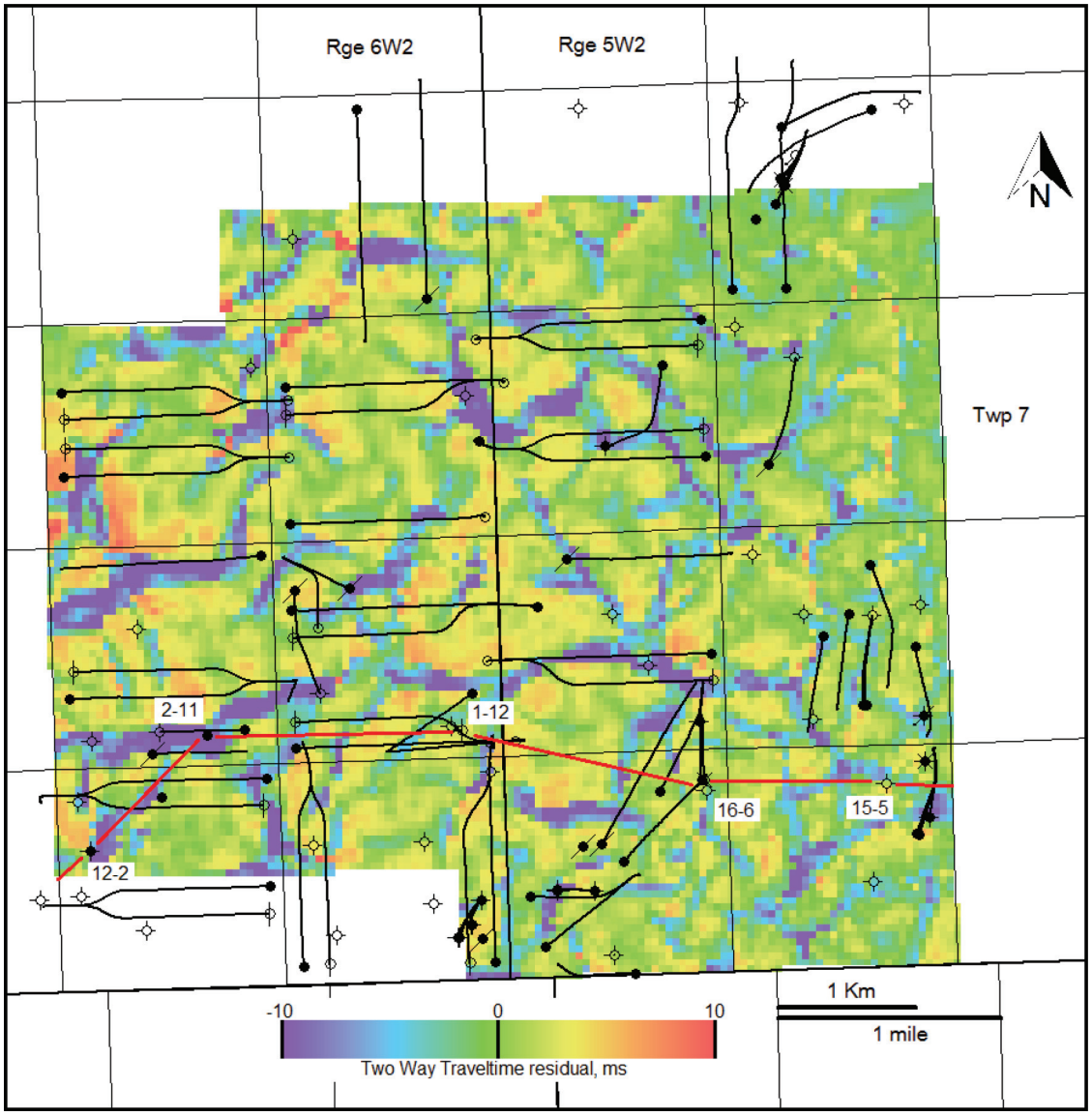

result of strike-slip movement between two well-defined wrench faults. In contrast, any shallow faulting observed interpreting these datasets appeared extensional in nature, and wrench faulting has not been observed.

The reason for the graben formation in an area without observed wrench faulting would have to be extensional tectonics on a local or regional scale. One possible explanation for local extension would be the movement of the backbulge associated with the Western Interior foreland system (Catuneanu 2004). The alignment of grabens suggests a paleostress field. To state that this would be occurring on a regional scale should only be made after the examination of data that expand this study area. For example, Johnson (2016) reports on a similar PFS system in the Pierre Shale, with a PFS and overlying graben system, in the Powder River Basin, Wyoming. Sonnenberg and Underwood (2012) have interpreted a Niobrara PFS with the Denver Basin. Here, the Niobrara appears to be faulted into grabens as well. I believe that these anomalies are all contained within one large PFS.

There are a few implications for a Late Cretaceous PFS and graben system in southeast Saskatchewan. A lot of shallow faults are implied by the fault densities discussed here, especially for the PFS. An area of 300 000 km² — well within the bounds of Saskatchewan and the Pierre Shale depositional area (Fig. 1) — would imply about 3 000 000 faults in Saskatchewan alone. This implication alone warrants that the GPPFS be studied further.

Anna and Cook (2008) examined the Niobrara Formation as a continuous petroleum system. They identified production "sweet spots" within Cretaceous sediments in the Great Plains area that coincided with surface lineaments that were assumed to be associated with zones of structural deformation and associated enhanced secondary porosity and permeability. The faulting presented here was not correlated to surface features such as lineaments. However, the PFS fault characteristics should be considered when examining hydraulic conductivity within the Great Plains area. Also, a U.S. Geological Survey (USGS) hydrogeological study (Anna 2011) examined the effects of groundwater flow on biogenic gas accumulations in the Great Plains area. The study was a finite element model that was built using permeability measurements from well control. There was no mention of modelling open or closed faults in situ in the analysis. Including PFS faulting in the model using different permeabilities along the PFS faults may (1) help the model and (2) help to determine if the faults in the subsurface are open or closed.

Fig. 14. Fault strike length and strike directions for the four main seismic reflections. The fault alignment on the Niobrara and the l. Campanian seismic reflections is absent on the shallower reflections. *n*, number of observations.

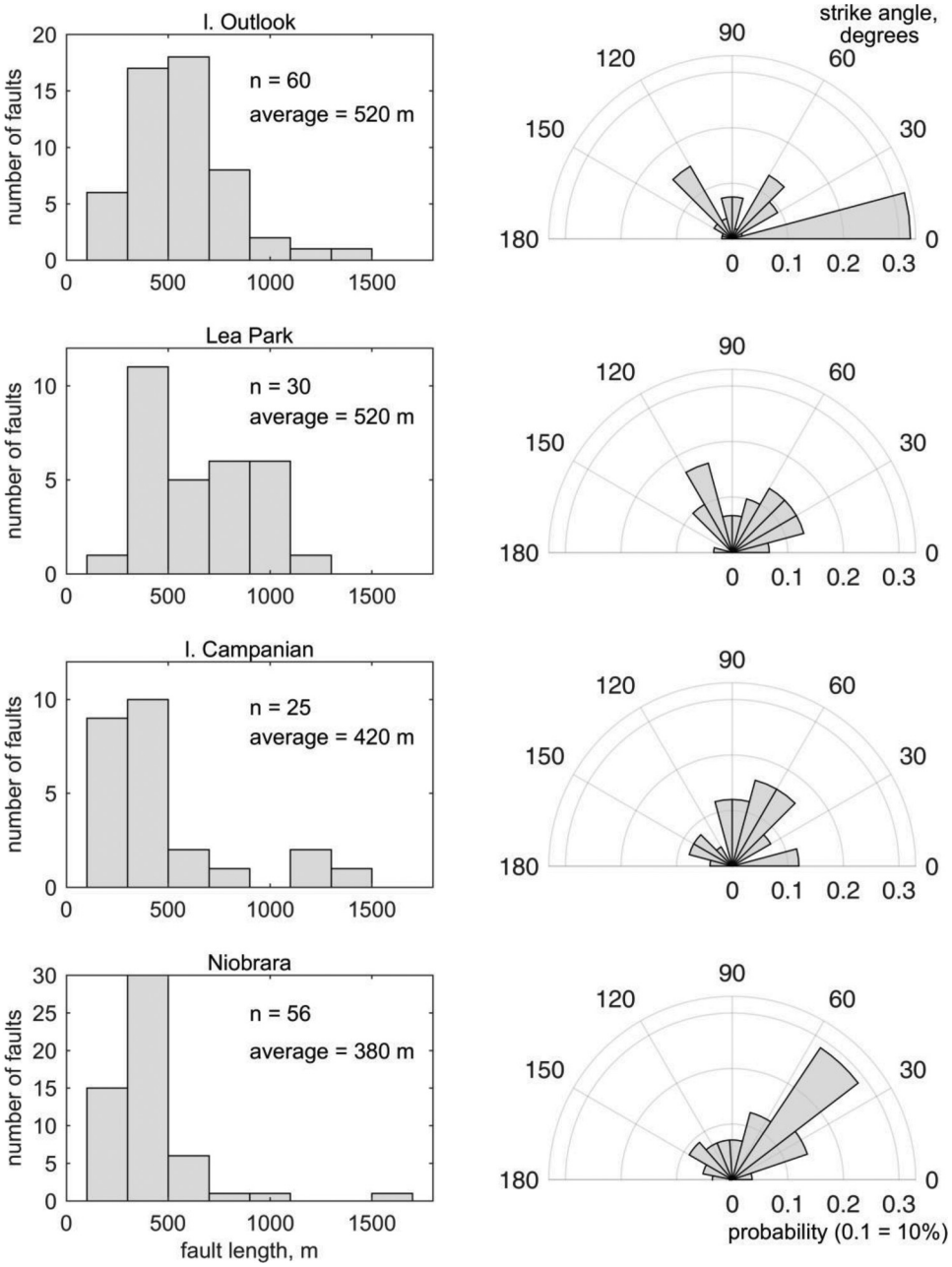

Although most potable water wells in southeast Saskatchewan source water from Tertiary and younger sediments, water test wells have been drilled into the Pierre Shale in southeast Saskatchewan (Saskatchewan Water Security Agency, available from www.wsask.ca, accessed on 22 July 2016). Water well productivity could be affected by encountering a subsurface fault. Work to investigate this possibility is recommended for future research.

Faulting at surface has been noted in Saskatchewan but has been attributed to processes other than PFS or Late Cretaceous grabens. Penner and Cosford (2010) looked at evidence linking surface lineaments with deeper horizons such as reactivated basement faults. However, there is a quiescent 2WS surface on most seismic data in southeast Saskatchewan, including the dataset studied here. This is indicating that deeper anomalies such as basement faults would not be expressed at surface. Moreover, Penner and Cosford (2010) make no mention of the structural variations in the Upper Cretaceous sediments such as those discussed here.

Late Cretaceous sediments are productive in many parts of the United States and Canada as a shallow, low-permeability oil and gas reservoirs. For example, the Tiger Ridge Field in Montana has produced natural gas from the Eagle Sandstone (Milk River homotaxial equivalent) since its discovery in 1966. Inks et al. (2010) reported on the aid of 3-D seismic in evaluating the pool for infill drilling potential. Mapping these areas for evidence of PFS and graben formation such as those presented here could help in understanding the reservoir geology.

The final point to be made with this communication is that the GPPFS has affected a volume of Late Cretaceous sediments within a very large area (Fig. 1). The variation in the correlations shown in Fig. 15 can be explained by simple, yet pervasive normal faulting within fine-grained sediments. The PFS can explain the occur-

Fig. 15. Comparison of the resistivity logs for the two wells at 16-6-7-5W2 and 15-5-7-5W2 from surface casing (where the logging begins) to just below the lower Campanian. The 15-5-7-5W2 resistivity log was separated into intervals that were adjusted to match the similar interval depth for 16-6-7-5W2. No stretching was applied to either log.

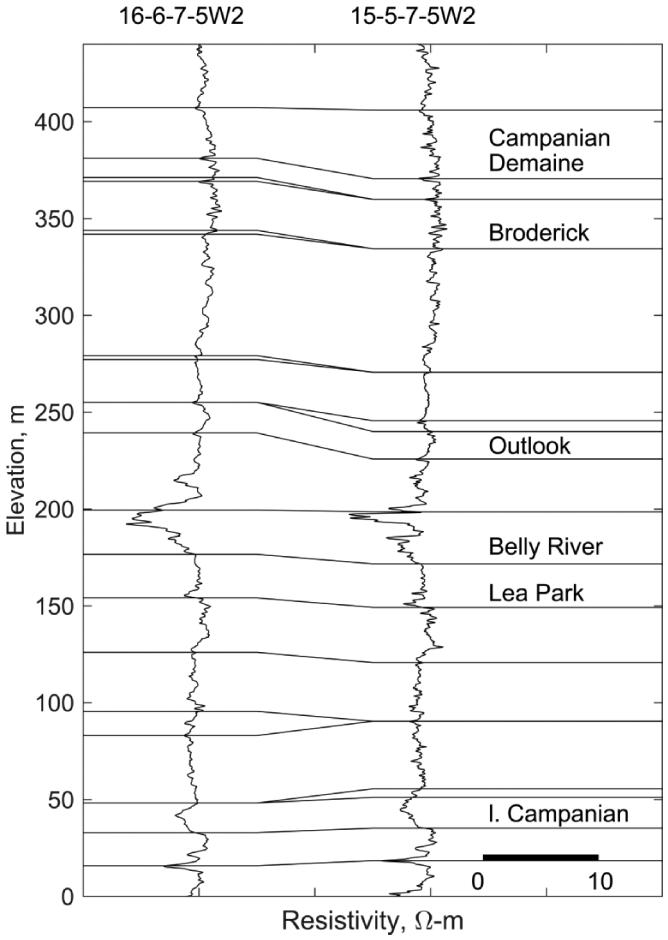

rence of shallow faults, variation in bed thickness, and missing section that is apparent on the simple two-well cross section.

Conclusions

A 3-D seismic survey from Saskatchewan has shown some characteristics of the GPPFS. This paper has shown the interpretation of a 3-D dataset from the GPPFS. Coniacian time normal faults were initiated over a Viking Formation channel sandstone, although direct measurement of drape compaction was not observed. These faults subsequently affected the PFS fault pattern in late Colorado and Pierre Shale Group sediments. Some of the PFS faulting continued to a Campanian clinoform sequence, where a graben system was identified. Four consistent seismic reflections mapped changes in fault strike direction and length, with vertical offset always increasing with the shallower beds. The fault timing, considered to have started shortly after deposition and terminated up to dates as late as the Tertiary, was aided by a number of wells drilled within the boundary of the seismic data.

Acknowledgements

The comments provided by Peter St-Onge and three anonymous reviewers are appreciated.

References

Anna, L.O. 2011. Effects of groundwater flow on the distribution of biogenic gas in parts of the northern Great Plains of Canada and United States. *In* U.S. Geological Survey Scientific Investigations Report 2010–5251, 24 p. https://pubs.usgs.gov/sir/2010/5251/pdf/sir2010-5251.pdf.

Anna, L.O., and Cook, T.A. 2008. Assessment of the Mowry Shale and Niobrara Formation as continuous hydrocarbon systems, Powder River Basin, Montana and Wyoming. *In* American Association of Petroleum Geologists Section Conference, July 9, 2008, Denver, Colo.: U.S. Geological Survey Open-File Report 2008–1367, 1 sheet.

Anna, L., Pollastro, R., and Gaswirth, S. 2010. Williston Basin Province—Resources in Assessment of Undiscovered Oil and Gas Resources of the Williston Basin Province of North Dakota, Montana, and South Dakota. U.S. Geological Survey Williston Basin Province Assessment Team, U.S. Geological Survey Digital Data Series DDS-69-W. Available from https://pubs.usgs.gov/dds/dds-069/dds-069-w/ [accessed 18 June 2016].

Bellahsen, N., and Daniel, J. 2005. Fault reactivation control on normal fault growth: an experimental study. Journal of Structural Geology, **27**: 769–780. doi:10.1016/j.jsg.2004.12.003.

Bertog, J. 2010. Stratigraphy of the lower Pierre Shale (Campanian): implications for the tectonic and eustatic controls on facies distributions. Journal of Geological Research: 910243. doi:10.1155/2010/910243.

Blakey, R. 2014. Paleogeography and Geologic Evolution of North America. Arizona, USA. Available from http://cpgeosystems.com/nam.html [accessed 15 April 2016].

Bloch, J., Schröder-Adams, C., Leckie, D., Craig, J., and McIntyre, D. 1999. Sedimentology, micropaleontology, geochemistry, and hydrocarbon potential of shale from the Cretaceous Lower Colorado Group in western Canada. Geological Survey of Canada Bulletin, **531**. Available from http://geoscan.nrcan.gc.ca/starweb/geoscan/servlet.starweb?path=geoscan/fulle.web&search1=R=211004 [accessed 26 November 2016].

Carruthers, D., Cartwright, J., Jackson, M., and Schutjens, P. 2013. Origin and timing of layer-bound radial faulting around North Sea salt stocks: New insights into the evolving stress state around rising diapirs. Marine and Petroleum Geology, **48**(2013): 130–148. doi:10.1016/j.marpetgeo.2013.08.001.

Cartwright, J. 1994. Episodic basin-wide hydrofracturing of overpressured early Cenozoic mudrock sequences in the North Sea Basin. Marine and Petroleum Geology, **28**: 587–607. doi:10.1016/0264-8172(94)90070-1.

Cartwright, J. 2011. Diagenetically induced shear failure of fine-grained sediments and the development of polygonal fault systems. Marine and Petroleum Geology, **28**: 1593–1610. doi:10.1016/j.marpetgeo.2011.06.004.

Cartwright, J. 2014. Are outcrop studies the key to understanding the origins of polygonal fault systems? Geology, **42**(6): 559–560. doi:10.1130/focus062014.1.

Cartwright, J., and Dewhurst, D. 1998. Layer-bound compaction faults in fine-grained sediments. Geological Society of America Bulletin, **10**(10): 1242–1257. doi:10.1130/0016-7606(1998)110<1242:LBCFIF>2.3.CO; 2.

Cartwright, J., and Lonergan, L. 1996. Volumetric contraction during the compaction of mudrocks: a mechanism for the development of regional-scale polygonal fault systems. Basin Research, **8**(2): 183–193. doi:10.1046/j.1365-2117.1996.01536.x.

Cartwright, J.A., Huuse, M., and Aplin, M.C. 2007. Seal bypass systems. American Association of Petroleum Geologists Bulletin, **91**(8): 1141–1166. doi:10.1306/04090705181.

Cartwright, J.A., James, D.M.D., and Bolton, A. 2003. The genesis of polygonal fault systems: a review. *In* Subsurface Sediment Mobilization. *Edited by* P. Van Rensbergen, R.R. Hillis, A.J. Maltman, and C.K. Morley. Geological Society, London, Special Publications, **216**: 223–243. doi:10.1144/GSL.SP.2003.216.01.15.

Catuneanu, O. 2004. Retroarc foreland systems – evolution through time. Journal of African Earth Sciences, **38**: 225–242. doi:10.1016/j.jafrearsci.2004.01.004.

Christopher, J.E., and Yurkowski, M. 2004. Geological mapping of Mesozoic strata in southeastern Saskatchewan, northwestern North Dakota, and northeastern Montana, and regional effects of deformation by glacial-ice loading. *In* Summary of Investigations 2004, Volume 1, Saskatchewan Geological Survey, Sask. Industry Resources, Misc. Rep. 2004-4.1. Available from http://economy.gov.sk.ca/adx/aspx/adxGetMedia.aspx?DocID=11842,11458,11455,11228,3385,5460,2936,Documents&MediaID=36620&Filename=chris.pdf [accessed 9 July 2016].

Christopher, J.E., Yurkowski, M., Nicolas, M., and Bamburak, J. 2006. The Cenomanian–Santonian Colorado formations of eastern southern Saskatchewan and southwestern Manitoba. *In* Saskatchewan and Northern Plains Oil & Gas Symposium 2006. *Edited by* C.F. Gilboy and S.G. Whittaker. Saskatchewan Geological Society Special Publication, **19**: 299–318, Available from http://www.gov.mb.ca/iem/petroleum/pubcat/Christopher_et_al.pdf [accessed 22 July 2016].

Cochran, A. 1991. Compaction and porosity prediction in chert-rich sandstones and conglomerates. AAPG Search and Discovery Article #91004, 1991 AAPG Annual Convention, Dallas.

Davies, J.J., Ireland, M.T., and Cartwright, J.A. 2009. Differential compaction due to the irregular topology of a diagenetic reaction boundary: a new mechanism for the formation of polygonal faults. Basin Research, **21**(3): 354–359. doi:10.1111/j.1365-2117.2008.00389.x.

Fischer, D., and Bluemle, J. 1986. Oil exploration and development in the North Dakota Williston Basin: 1984–1985 update, North Dakota Geological Survey, Miscellaneous Series No. 67. Available from https://www.dmr.nd.gov/ndgs/documents/Publication_List/pdf/MiscSeries/MS-67.pdf [accessed 18 June 2016].

Gendzwill, D., and Stauffer, M. 2007. Shallow faults, Upper Cretaceous clinoforms, and the Colonsay Collapse, Saskatchewan. Canadian Journal of Earth Sciences, **43**(12): 1859–1875. doi:10.1139/e06-071.

Goulty, N., and Swarbrick, R. 2008. Development of polygonal fault systems: a test of hypotheses. Journal of the Geological Society, London, **162**: 587–590. doi:10.1144/0016-764905-004.

Hack, J.T. 1973. Drainage adjustment in the Appalachians. *In* Fluvial geomorphology. *Edited by* M. Morisawa. Publications in Geomorphology, Binghamton, New York, State University of New York, pp. 51–69.

Hampson, G.J. 2010. Sediment dispersal and quantitative stratigraphic architecture across an ancient shelf. Sedimentology, **57**: 96–141. doi:10.1111/j.1365-3091.2009.01093.x.

Henriet, J.P., Batist, M., and Verschuren, M. 1991. Early fracturing of Paleogene clays, southernmost North Sea: Relevance to mechanisms of primary hydrocarbon migration. *In* Generation, Accumulation and Production of Europe's Hydrocarbon. *Edited by* A.M. Spencer. Special Publications of the European Association of Petroleum Geologists, **1**: 217–227.

Inks, T., Baclawski, P., Seaton, C., and Estes, S. 2010. Productive wrench grabens imaged on 3D seismic, Tiger Ridge Field, Blaine and Hill Counties, Montana. AAPG Search and Discovery Article #20083.

Jackson, C., Carruthers, D., Mahlo, S., and Briggs, O. 2014. Can polygonal faults help locate deep-water reservoirs? American Association of Petroleum Geologists Bulletin, **98**(9): 1717–1738. doi:10.1306/03131413104.

Johnson III, W. 2016. 3D seismic interpretation of polygonal faulting in Upper Cretaceous sediments, Powder River Basin, Wyoming. M.Sc. Thesis, The University of Texas at San Antonio. Available from http://gradworks.umi.com/10/10/10108487.html [accessed 24 July 2016].

Lopez, T., Antoine, R., Darrozes, J., Rabinowicz, M., and Baratoux, D. 2015. Formation of polygonal fracture system as a result of hydrodynamic instabilities in clay-rich deposits. Geological Society of America Annual Meeting, Baltimore, Maryland. Available from https://gsa.confex.com/gsa/2015AM/webprogram/Handout/Paper267450/Poster_Clays_GSA15.pdf [accessed on April 16, 2016].

Maher, H. 2014. Distributed normal faults in the Niobrara Chalk and Pierre Shale of the central Great Plains of the United States. Lithosphere, **6**(5): 319–334. doi:10.1130/L367.1.

Mattos, N.H., Alves, T., Marcos,•Omosanya, K.O. 2016. Crestal fault geometries reveal late halokinesis and collapse of the Samson Dome, Northern Norway: Implications for petroleum systems in the Barents Sea. Tectonophysics, **690A**: 76–96. doi:10.1016/j.tecto.2016.04.043.

Nurhasan, A., and Davis, T. 2016. Interpretation of wrench faulting and fault related pressure compartmentalization, Wattenberg Field, Denver Basin Colorado. EAGE First Break, **34**(2): 53–61.

Patruno, S., Hampson, G., and Jackson, C. 2015. Quantitative characterisation of deltaic and subaqueous clinoforms,. Earth-Science Reviews, **142**: 79–119. doi:10.1016/j.earscirev.2015.01.004.

Penner, L., and Cosford, J. 2010. Evidence linking surface lineaments and deep-seated structural features in the Williston basin. *In* Saskatchewan and Northern Plains Oil & Gas Symposium 2006. *Edited by* C.F. Gilboy and S.G. Whittaker. Saskatchewan Geological Society Special Publication, **19**: 19–39.

Reeve, M., Bell, R., Duffy, O., Jackson, C., and Sansom, E. 2015. The growth of non-colinear normal fault systems; what can we learn from 3D seismic reflection data? Journal of Structural Geology, **70**: 141–155. doi:10.1016/j.jsg.2014.11.007.

Roberts, L., and Kirschbaum, M. 1995. Paleogeography of the Late Cretaceous of the Western Interior of Middle North America- Coal distribution and sediment accumulation. USGS Professional Paper 1561, US Government Printing Office. Available from http://pubs.usgs.gov/pp/1561/report.pdf [accessed 16 April 2016].

Schröder-Adams, C.J., Cumbaa, S.L., Bloch, J., Leckie, D.A., Craig, J., Seif El-Dein, S.A., et al. 2001. Late Cretaceous (Cenomanian to Campanian) paleoenvironmental history of the Eastern Canadian margin of the Western Interior Seaway: bonebeds and anoxic events. Palaeogeography, Palaeoclimatology, Palaeoecology, **170**: 261–289. doi:10.1016/S0031-0182(01)00259-0.

Schultz, L., Tourtelot, H., Gill, J., and Boerngen, J. 1980. Composition and properties of the Pierre Shale and equivalent rocks, northern Great Plains region. USGS Professional Paper 1064. Available from http://pubs.usgs.gov/pp/1064b/report.pdf [accessed 15 April 2016].

Simpson, M. 1993. Geology and groundwater resources of the Weyburn/Virden Area (62E/F), Saskatchewan. Available from https://www.wsask.ca/Global/Water%20Info/Ground%20Water/Mapping/Estevan%20Mapsheet%2062EF/Reports/R12103E93.pdf [accessed 22 July 2016].

Sonnenberg, S.A., and Underwood, D.F. 2012. Polygonal fault systems – a new structural style for the Niobrara Formation and Pierre Shale, Denver Basin, Colorado. AAPG Search and Discovery Article # 50624 (2012). Available from http://www.searchanddiscovery.com/documents/2012/50624sonnenberg/ndx_sonnenberg.pdf [accessed November 2016].

St-Onge, A. 2016. A Late Cretaceous polygonal fault system in central North America. Geological Society of America Bulletin, in review.

Tewksbury, B., Hogan, J., Kattenhorn, S., Mehrtens, C., and Tarabees, E. 2014. Polygonal faults in chalk: Insights from extensive exposures of the Khoman Formation, Western Desert, Egypt. Geology, **42**(6): 479–482. doi:10.1130/G35362.1.

Walz, C., and Pederson, P. 2013. Petrographic, stable isotope and fluid inclusion characteristics of the Viking sandstones: implications for sequence stratigraphy, Bayhurst area, SW Saskatchewan, Canada. *In* Linking Diagenesis to Sequence Stratigraphy. *Edited by* S. Morad, J.M. Ketzer, and L.F. De Ros. John Wiley & Sons, Inc., Chapter 14, West Sussex, UK. doi:10.1002/9781118485347.ch14.

Weimer, R. 1960. Upper Cretaceous Stratigraphy, Rocky Mountain area. American Association of Petroleum Geologists Bulletin, **44**(1): 1–20.

Witzke, B.J., and Ludvigson, G.A. 1994. The Dakota Formation in Iowa and the type area. *In* Perspectives on the Eastern Margin of the Cretaceous Western Interior Basin. *Edited by* G. Shurr, G. Ludvigson, and R. Hammond. Geological Society of America Special Papers, **287**: 43–78. doi:10.1130/SPE287-p43.

Zhou, B., and Hatherly, P. 2014. Fault and dyke detectability in high resolution seismic surveys for coal: a view from numerical modelling. Exploration Geophysics, **45**(3): 223–233. doi:10.1071/EG12082.